

**Interpreting the Subsurface Geology beneath the  
Ross Ice Shelf, West Antarctica,  
using Airborne Gravity and Magnetic data**

A Senior Thesis presented to  
The Faculty of the Department of Geology

SUBMITTED IN PARTIAL FULLFILLMENT OF THE REQUIREMENTS FOR THE  
DEGREE OF BACHELOR OF ARTS

Alec C. Lockett  
The Colorado College  
May 2017

## Table of Contents

List of Figures	3
List of Tables	3
Abstract	4
Introduction	5
Background on Geological and Geophysical Features	8
Previous Investigations	11
Methods	16
i.    2016 Data Collection	17
ii.   Data Management and Modeling Software	20
Data	21
Modeling	23
Discussion	33
i.    Geophysical Modeling	33
ii.   Confidence of Constraints from Modeling	35
iii.  Regional Implications	37
Conclusion	41
Figures	43
References	66

## List of Figures

Figure 1	43
Figure 2	44
Figure 3	45
Figure 4	46
Figure 5	47
Figure 6	48
Figure 7	49
Figure 8	50
Figure 9	51
Figure 10	52
Figure 11	53
Figure 12	54
Figure 13	55
Figure 14	56
Figure 15	57
Figure 16	58
Figure 17	59
Figure 18	60
Figure 19	61
Figure 20	62
Figure 21	63
Figure 22	64
Figure 23	65

## List of Tables

Table 1	14
Table 2	14-15
Table 3	24

## Abstract

The bathymetry beneath the Ross Ice Shelf in West Antarctica controls the circulation of sub-shelf ocean water that may warm the ice shelf from below, with consequences for shelf stability and climate warming. Thick ice and underlying seawater obscure the seafloor, which is why the bathymetry cannot be measured directly and is only crudely known. The program Oasis Montaj (GeoSoft ©) is used to manage geophysical datasets within a geospatial framework and its extension, GM-SYS, is used to model geological profiles in an iterative process by inserting polygons and assigning various densities and magnetic susceptibilities to produce a calculated fit for the observed geophysical data. Grid and point geophysical data come from ROSETTA-Ice's 2015-2016 survey. Imported into Oasis Montaj, the data along two transects were used to constrain the geologic makeup of 2D crustal profiles using the software GM-SYS. These data are used together with geological information and geophysical parameters from the bordering region of Marie Byrd Land, the Ross Sea, and the Transantarctic Mountains. The two cross-shelf transects are survey lines 310 and 720. Line 310 is of interest because it crosses an elevated portion of the grounding line between shelf ice that is floating and grounded ice on land. Known as Crary Ice Rise, the elevated region may be controlled by faults. Line 720 spans about 600 kms across the northern part of the shelf, crossing Roosevelt Island and a narrow trough that might be fault controlled or glacially carved.

Line 310 exhibits several short wavelength, high amplitude magnetic anomalies as well as a single short wavelength anomaly of even higher amplitude, but is dominated by long wavelength, low amplitude anomalies. The range of values is -2380 nT to -2040 nT. Gravity data is characterized by long wavelength, moderate amplitude anomalies, and yields a range of values from -67 mgal to -16 mgal. Line 720 shows moderate to long wavelength, small amplitude anomalies, and a group of short wavelength, high amplitude anomalies in close proximity. The profile has a range of values from -2382 nT to -2080 nT. Apart from one moderate wavelength, high amplitude feature, anomalies with very long wavelengths and weak amplitudes comprise the gravity signature. Values range from -78 mgal to 10 mgal. In both transects, steep geophysical gradients align with the margins of 'bathymetric' features in the depth to magnetic basement map. Initial models include an average crustal density of  $2.67 \text{ g/cm}^3$  and a standard mantle density of  $3.3 \text{ g/cm}^3$ . Magnetic susceptibilities for the average crust range from 0.0001 K to 0.000075 K, based on values reported in previous studies or measured from hand samples. Large polygons with densities of about  $3.0 \text{ g/cm}^3$  and susceptibilities of about 0.013 K beneath a  $2.4 \text{ g/cm}^3$  layer improved the fit between the calculated and observed curves. Small horizontal sectors with a density of  $2.5 \text{ g/cm}^3$  and susceptibilities ranging from 0.001 K to 0.008 K resolved anomalies with weak gravity signatures coupled with intermediate magnetic signatures.

Modelling of gravity and magnetic data together reveal critical geological elements beneath the shelf such as sedimentary basins, large deep-sourced intrusions –

some of which sit below basin depocenters, mafic dike arrays, and sills of intermediate susceptibilities. Based on these interpretations, it is likely that Crary Ice Rise is controlled by normal faulting, which influences glacier dynamics at the grounding line. Mafic intrusions present in the subsurface probably reflect past rifting and consequently an elevated Moho depth. Both transects 310 and 720 exhibit a prominent shift in magnetic anomalies midway across the shelf. This transition marks a possible lithospheric boundary between East and West Antarctica. This new crustal boundary has consequences for the shape, depth, and roughness of the seabed, as well as for plate structure and dynamics.

## Introduction

The Ross Ice Shelf (RIS) is a floating extension of the West Antarctic Ice Sheet that occupies the southern Ross Embayment in West Antarctica (Figure 1). Bounded by the Transantarctic Mountains (TAM) to the southwest and by Marie Byrd Land to the north, the ice shelf contains ice coming from ice streams that flow from West Antarctica and outlet glaciers that transect the TAM. The ice shelf acts as a buttress to the Antarctic ice sheets, making it a key element in modeling of climate warming scenarios. However, the bathymetry beneath the shelf, which controls the circulation of sub-Shelf ocean water that may warm the Ice Shelf from below, is unknown (*Jacobs et al.*, 2011; *Joughin et al.*, 2005; *Peters et al.*, 2006; *Rignot et al.*, 2014). Thus, it is difficult to model shelf stability in deglaciation scenarios. Thick ice and underlying seawater obscure the seafloor beneath the Ross Ice Shelf which is why the crustal makeup and seabed bathymetry are very poorly known, from only sparse RIGGS<sup>1</sup> data (Figure 2). The sub-RIS bathymetry cannot be measured directly. Rather, the bathymetry must be determined through the use of geophysical data— gravity and magnetic data, specifically—to determine the subsurface geology, which can then be applied to interpretations of the probable bathymetry beneath

---

<sup>1</sup> Ross Ice Shelf Geophysical Glaciological Survey

the Shelf. The subsurface geology can be constrained by airborne gravity and magnetic data, that reflect the size, type, and origin of geological features, such as igneous bodies or fault zones. Sparse depth-sounding data from the 1970's RIGGS provide control points for bathymetry (Figure 3; *Bentley et al.*, 1981).

ROSETTA-Ice (a systems approach to understanding the Ross Ocean and Ice Shelf Environment, and Tectonic setting Through Aerogeophysical surveys and modeling) is a current project that is acquiring geophysical data over the Ross Ice Shelf through airborne collection (Figure 2; *Bell et al.*, 2014). For my senior research, I used airborne gravity and magnetic data from the ROSETTA-Ice 2015-2016 surveys to model the geological makeup of two cross-RIS transects using Oasis Montaj software (GeoSoft ©). Geological and geophysical information from the bordering region of Marie Byrd Land, where there are extensive rock exposures, provide a baseline for decisions about the makeup of the crust beneath the Ross Ice Shelf. Grounded ice regions contain potential fault zones (*Muto et al.*, 2013; *Elkind et al.*, 2016) and igneous centers (*Behrendt et al.*, 2007) that may correspond to areas of elevated geothermal heat that influence ice shelf stability.

I selected two Ice Shelf transects for modeling of the geology of the crust, using gravity and magnetic data from ROSETTA-Ice's 2015-2016 survey (Figure 2). One transect along the flight **line 310** (~350 km length) passes along the grounding line and bedrock highs including the Crary Ice Rise. Prospectively, the rises are controlled by faults formed during repeated rifting in the Ross Embayment (*Muto et al.*, 2013).

The flight **line 720 transect** (~600 km length) extends from the Transantarctic Mountains and passes the southern tip of Roosevelt Island east to western Marie Byrd

Land, and includes prominent geophysical anomalies. It also includes crustal troughs on either side of Roosevelt Island that align with basins in the Ross Sea. For geophysical modeling, only the eastern half of the transect was considered.

The transects afford the opportunity to address the following questions:

- Do magnetic and gravity anomalies reveal geological structures that could be related to features/fabrics known from ground observations in Marie Byrd Land?
- Based on magnetic and/or gravity properties, what rock types characterize the bedrock and what are their origins?
- Is there evidence for sedimentary basins and/or thick subglacial sediment packages of fairly low density, that may reflect rift basins or deposits from the West Antarctic Ice Sheet? If present, could these possibly aid the flow of ice streams?
- What implications do the presence or absence of these features have for the oceanographic circulation and the stability of the Ross Ice Shelf? What do these features reveal about the regional tectonic history?

Gravity and magnetics models of flight lines 310 and 720 (east), created using Oasis Montaj, will improve our understanding of the concealed bedrock geology influencing the Ross Ice Shelf and contribute interpretations that are critical to the task of modeling Ross Ice Shelf bathymetry. Therefore, the research has bearing on the stability of the Ice Shelf and its contribution to climate warming. New insights into the makeup of Earth's crust will lead to a greater understanding the tectonic history of the region.

## Background on Geological and Geophysical Features

The Ross Embayment is the portion of West Antarctica that contains the Ross Sea and Ross Ice Shelf (Figure 1). The West Antarctic Ice Sheet overlies West Antarctica and is rapidly changing due to climate warming (*Rignot et al.*, 2014). The WAIS undergoes dynamic change partially because it rests upon a complex tectonic province made up of terranes, that has been affected by Cretaceous to Present regional extension and volcanism. West Antarctica includes Marie Byrd Land, the Ross Embayment, the Antarctic Peninsula, the Ellsworth Mountains and the Weddell Sea, and is bounded on the interior by the Transantarctic Mountains. The history of formation and filling of extensional basins (*Decesari et al.*, 2007) in the Ross Sea might pertain to the region beneath the Ross Ice Shelf. The Shelf region is only minimally known from the 1970s RIGGS survey (*Bentley et al.*, 1981), which proposed the existence of prominent bedrock highs and sediment-poor troughs, with a comparatively low volume of glacial sediments (Figure 2; *Bell et al.*, 2014 proposal).

The Ross Sea includes three major tectonic basins, the Victoria Land Basin, the Central Trough, and the Eastern Basin, with two basement highs, the Coulman and Central High, which separate the structural basins (Figure 4). Marine sedimentary sequences imaged by seismic reflection in the Eastern Basin and Roosevelt Sub-basin (Figure 5; *Sorlien et al.*, 2007) are RSS-7&8 (Plio-Pleistocene), RSS-5 (unknown), RSS-4 (Lower-Mid Miocene), RSS-3 (Lower Miocene), RSS-2 (Oligocene-Miocene), and RSS-1 (unknown). The sequences are characterized by broad troughs that have been filled during ice retreat and renewed during ice advance. Sedimentary layers contain a record of changes in the West Antarctic Ice Sheet over the Ross Sea.

The bathymetry of the Ross Sea is known from oceanographic surveys (Figure 4; *Davey et al.*, 2016; *Decesari et al.*, 2007; *Karner et al.*, 2005; *Luyendyk et al.*, 2003; *Wilson and Luyendyk*, 2006). Elongate highs and broad lows are constituted of voluminous glacial drift. In contrast, the bathymetry of the Ross Ice Shelf is poorly known because remote sensing through thick floating ice is not straightforward. A valuable legacy dataset comes from the RIGGS survey conducted between 1973-1974 and 1977-1978, in which water depths were calculated at stations spaced 55 km apart. Interpolation between RIGGS points produced a low resolution bathymetric map (*Bentley et al.*, 1981) that is incorporated in BEDMAP2 (*Fretwell et al.*, 2013). BEDMAP2 portrays bathymetry beneath the Ross Ice Shelf to be <1000 mbsl with a few wide areas reaching <500 mbsl, suggestive of nearly flat bedrock platforms separated by deep troughs.

The rock units underlying much of Marie Byrd Land likely continue beneath the Ross Ice Shelf, based on the established continuity of formations between Gondwana convergent margin terranes (*Siddoway et al.*, 2004; *Siddoway*, 2008; *Elkind et al.*, 2016). The oldest of these in Marie Byrd Land is the Swanson Formation, consisting of Cambrian-Ordovician turbidites. I-type plutons and granites (Ford Plutonic Suite) intruded the Swanson Formation at ~375-345 Ma during convergent arc magmatism (*Pankhurst et al.*, 1998; *Yakymchuk et al.*, 2015). The Byrd Coast Granite suite in western Marie Byrd Land was emplaced in Middle Cretaceous time during regional A-type plutonism, the granites a product of melting of lower middle crust (*Siddoway*, 2008). The Ford Ranges consists mainly of the early Paleozoic Swanson Formation and Ford Granodiorite. A metamorphic core complex hosting a gneiss dome is found in the

Fosdick Mountains, providing evidence of large extension (*McFadden et al.*, 2010; *Siddoway*, 2008, 2016). The dome is bounded by the Balchen Glacier fault, the existence of which is supported by distinct thermal histories, AMS fabrics (*Siddoway et al.*, 2004), and steep gravity and magnetic gradients (*Luyendyk et al.*, 2003). The West Antarctic crust is dramatically thin (*Chaput et al.*, 2014); therefore it is likely that other core complexes exist and can be identified on the basis of their geophysical expression, for example, along the proposed research transects 310 and 720. Further east of the survey line 720 into western Marie Byrd Land and the Ford Ranges, several gravity model profiles have been published which use data from the SOAR (Support Office for Aerogeophysical Research at the University of Texas, Austin) survey (*Luyendyk et al.*, 2003). These models are geologically simple, assigning a single uniform density for supracrustal sediments and one for the entire crust; profiles are based on free air gravity anomalies, without specific use of magnetic anomaly data (*Luyendyk et al.*, 2003). Structural data exist and kinematic analysis has also been conducted in the Ford Ranges (*Luyendyk et al.*, 2003). All of the known geology of western Marie Byrd Land and the Ford Ranges, that lie east of line 720, has been compiled into a digital subglacial geologic map (*Elkind et al.*, 2016; *Siddoway et al.*, 2016).

The majority of crustal thinning in West Antarctica occurred during Cretaceous intracontinental extension across West Antarctica and Zealandia (comprising the islands of New Zealand and contiguous large regions of submerged continental crust), which were contiguous at the time (*Siddoway*, 2016). Lower middle crust was exhumed in the Fosdick Mountains migmatite dome/core complex (*McFadden et al.*, 2010) and basin-and-range style features of the Ross Sea formed, including the Central High (*Fitzgerald*

*and Baldwin, 1997)* and the Colbeck Trough (*Siddoway et al., 2004*). These events reduced the crustal thicknesses attained during prior plate convergence (e.g. *Bialas et al., 2007*). Plateaus underly Edward VII Peninsula, and Siple Dome, Roosevelt Island, and Cape Colbeck coincide with surfaces that may have been formed by wave cut erosion after landscape stabilization in the Miocene (Figure 3; *Wilson and Luyendyk, 2006*).

Ongoing tectonism in Marie Byrd Land is reflected by Neogene age volcanism from 19 Ma to present, that produced large alkali basalt centers that rise through and above the West Antarctic Ice Sheet. They are distributed along chains that for middle-Late Miocene eruptions are mainly oriented north-south. Late Miocene-Pleistocene chains are aligned east-west, with isolated elongated volcanos also exhibiting an east-west orientation (*LeMasurier and Rocchi, 2005; Paulsen and Wilson, 2010*). There are likely to be volcanic centers or lineaments beneath the RIS survey region, that if present will display strong gravity and magnetic anomalies (*Behrendt et al. 2007*). Prospectively, active faults control prominent grounding line features such as the Roosevelt Sub-basin and Crary Ice Rise. The Crary Ice Rise is an elevated promontory along the grounding line in the southern Ross Ice Shelf (Figure 1). A steep gravity gradient detected from an on-ice survey suggests the presence of a fault at the mouth of the Whillans Ice Stream, that may continue and control the position of Crary Ice Rise (*Muto et al., 2013*).

### **Previous Investigations**

Gravity and magnetic data are incredibly useful tools for studying the geology of the crust because they can provide insight to the geometry, depth, and characterization of concealed rock bodies. Forward modeling of gravity and magnetic data together with an understanding of the regional geology then allows us to characterize the subsurface.

Airborne surveys using gravity and magnetics have been conducted over large regions of grounded ice that surround the RIS.

For the Ross Sea, marine surveys are numerous, with valuable, recent compilation datasets published in Karner et al., (2005) and Decesari et al., (2007). A notable paradox exists in the Ross Sea: positive gravity anomalies are associated with sedimentary basins. This was modeled by *Karner et al.*, (2005) with high-density intrusions beneath the basins. Considering these studies, structural profiles of the Ross Ice Shelf extending from the Fosdick Mountains to the Transantarctic Mountains have been created (*Siddoway et al.*, 2016) which depict deep sourced mafic bodies on graben floors.

The Central West Antarctica aerogeophysical survey (CWA) from 1990-1997 collected extensive aeromagnetic and radar data, and subsequent studies revealed numerous concentric, short-wavelength, high-amplitude magnetic anomalies that correspond to positive gravity anomalies (*Behrendt et al.*, 2007). These are interpreted as shallow source igneous centers (*Behrendt*, 2013), that might continue beneath the RIS.

The SOAR facility (Support Office for Aerogeophysical Research at the University of Texas, Austin) conducted airborne geophysical surveys across Transantarctic Mountain transects. and a portion of western Marie Byrd Land including the Ford Ranges and part of Edward VII Peninsula, from 1998-1999 (*Luyendyk et al.*, 2003; *Wilson and Luyendyk*, 2006). Magnetic and gravity data, as well as radar echo soundings to determine ice surface elevation and ice thickness, were collected over a region about 470 km by 350 km. During the GANOVEX VII expedition, aeromagnetic data were gathered over Edward VII Peninsula (*Ferraccioli et al.*, 2002). Collectively, these data were used to extend the geology known from rock exposures (*Siddoway et al.*, 2004) to the subglacial

environment (*Elkind et al.*, 2016). The regional geology for Marie Byrd Land is newly available as a digital geological map dataset in ArcGIS (*Elkind et al.*, 2016; *Siddoway et al.*, 2016) that consolidates all of the geological information for Marie Byrd Land in a geospatial framework that can be integrated with new geophysical data from ROSETTA-Ice. Aerogeophysical surveys inland of the TAM in East Antarctica (*Studinger et al.*, 2004) extending to the Ross Sea (*Goodge and Finn*, 2010) have also been conducted, and tectonic models of extension of the East Antarctic and West Antarctic crust have been proposed (*Beek et al.*, 1994; *Huerta and Harry*, 2004).

Using the ROSETTA magnetic dataset, the depth to sediment basement contact for the Ross Embayment has been determined by a Werner deconvolution method (Figure 6; *Wilner et al.*, 2016). Grids of columnar density and cover thickness were also created, revealing a paradoxical relationship: areas with high columnar density coincide with the greatest depth to magnetic basement and cover. Crustal troughs under the Ross Ice Shelf differ in the trend of Ross Sea crustal troughs and are associated with highs in the free-air gravity grid.

These previous aerogeophysical investigations provide a foundation for use of potential fields data to interpret the geology of the sub-Ross Ice Shelf. Drawing upon these studies, a tabulation of gravity and magnetic characteristics for known rock types is provided in Table 1. The direct measurements provide the range of values that may reasonably be used as characteristics in modeling in GM-SYS.

*Table 1: Characteristics for known formations in Marie Byrd Land. Measurements were compiled from various sources.*

Rock Type	Density (kg/m <sup>3</sup> )	Susceptibility (K)	Susceptibility (SI)	Gravity Signature	Magnetic Signature	Source
Swanson Formation	2600-2700	.000151	0.151	Moderate	Weak	<i>Ferraccioli et al., 2002; Luyendyk et al., 2003</i>
Ford Granodiorite	2670-2790	.000066	0.066	Moderate	Weak	<i>Ferraccioli et al., 2002</i>
Byrd Coast Granite	2520-2810	.003308	3.308	Weak-moderate	Moderately magnetic	<i>Ferraccioli et al., 2002</i>
Cenozoic Volcanics	2700-3300	.045	45.0	Strong	Highly magnetic	<i>Ferraccioli et al., 2002</i>
Migmatites-Edward VII Peninsula	2600-2900	.000152	0.152	Moderate	Weak-moderate	<i>Ferraccioli et al., 2002</i>
Migmatites-Alexandra Mountains	2600-2900	.009354	9.354	Strong	Highly magnetic	<i>Ferraccioli et al., 2002</i>
Ferrar Dolerite	2300-2500	$\leq .0008$	8.0	Weak	Weak-moderate	<i>Goodge and Finn, 2010</i>

*Table 2: Rock samples measured for density and magnetic susceptibility. Samples were collected from Ford Ranges outcrops.*

Sample	Rock Type	Density (kg/m <sup>3</sup> )	Susceptibility (K)	Susceptibility (SI)	Gravity Signature	Magnetic Signature
921-4	Greenland Group	2575	.00023	0.23	Moderate	Moderate
01222-B2 (a)	Kfs Granite	2452	.00008	0.08	Weak-Moderate	Weak
01222-B2 (b)	Kfs Granite	2772	.00007	0.07	Strong	Weak

01222-B2 (c)	Kfs Granite	2905	.00008	0.08	Strong	Weak
10125-5	Granite	2406	.00467	4.67	Weak-Moderate	Moderate
21220-4	Plagioclase + Biotite banded gneiss	2677	.00626	6.26	Moderate-Strong	Moderate-High
155	Gneiss	2672	.00026	0.26	Moderate-Strong	Moderate
III	Gneiss	2721	.00020	0.20	Moderate-Strong	Moderate
21223-9	Metasedimentary turbidite	2650	.00013	0.13	Moderate-Strong	Weak-Moderate
C6-BB106 (a)	Gneiss	2578	.00007	0.07	Moderate	Weak
C6-BB106 (b)	Gneiss	2593	.00011	0.11	Moderate	Weak-Moderate
P-12 (a)	Basalt	2167	.00221	2.21	Weak	Moderate
P-12 (b)	Basalt	2131	.00054	0.54	Weak	Weak

## Methods

Gravity and magnetic forces are potential fields, meaning that the strength and direction of the field depends on the position of observation. Generally, an area where material is less dense than the average crust will yield a low gravity anomaly, and one where material is denser will yield a higher gravity anomaly. Variations in lateral density produce gravity anomalies, which can be used with geologic knowledge of the region to constrain the nature of contact between different bodies of rock. The wavelengths of anomalies also provide information about the depth to the concealed body. Deep sourced bodies are usually associated with long wavelengths, while shallow or near surface bodies are typically correlated with small or short wavelengths. This is also true for magnetic anomalies, which result from variations in the distribution and strength of magnetic minerals that are a consequence of rock type. The degree to which a rock is magnetized is called magnetic susceptibility, and is a dimensionless unit that is found by multiplying the susceptibility of the magnetic mineral with the percentage of that mineral in the rock and divided by 100. Some minerals may be diamagnetic, which means their induced magnetization is in the opposite direction of the applied external field, resulting in a negative magnetic susceptibility. In areas of shallow Moho depth, it is reasonable to assume that the Curie depth would be elevated, and as a result the thickness of magnetized rock would be less than along segments where the crust is thicker. Variations in total magnetization produce magnetic anomalies, that are the sum of induced and remnant magnetization. Induced magnetization is caused by the present magnetic field of the earth and when the rock is removed from this ambient field, the magnetization can be lost. Remnant magnetization is the permanent magnetization that remains after the

ambient field changes. For example, when rocks lithify the orientation of magnetic domains of minerals stays in the direction of the magnetic field at the time of lithification. Although the total magnetic field is a vector sum of the ambient field and the induced magnetic field, to achieve the total field anomaly, only the magnitude of the ambient field is subtracted from the total magnetic field. The size, shape, depth and magnetic properties of a concealed body determine the type of magnetic anomaly (*Lillie, 1999*). The size, shape, and magnetic characteristics of crustal bodies are an objective of my thesis work.

ROSETTA-Ice uses instruments called gravimeters to measure changes in gravitational acceleration, by monitoring the sensitive responses of a mass suspended on a spring which is attached to a beam. As the earth's field changes, the force exerted on the spring by the mass varies, also changing position of the mass and the length of the spring; the change in spring length reflects the change in gravity (*Lillie, 1999*). For acquisition of new data along flight lines, ROSETTA-Ice uses three gravimeters (Figure 7) and IcePod (Figure 8), a suite of instruments that includes two magnetometers, visual and infrared camera, LiDar, deep ice radar (DEEP), shallow ice radar (SIR), and a PNT (position, navigation, and tracking) system that includes GNSS (global navigation satellite system) and IMU (inertial measurement unit), (Lamont-Doherty Earth Observatory). DEEP is being used primarily to detect ice sheet thickness, with ice penetration up to 1-2 kilometers (*Bell et al., 2014*).

### *2016 Data Collection*

I joined the on-ice team as part of the ROSETTA project in November and December, 2016, to participate in the collection of aerogeophysical data. New data were reviewed immediately after surveying to ensure the data are reasonable, quality, and that

instruments were working properly so that additional surveying may continue. After daytime flights, I downloaded the data from the gravimeters and after they were archived, quality checked the gravity and magnetic data using a MatLab script and Oasis Montaj. I examined several plots reflecting temperature, pressure, ellipsoid height, vertical acceleration, platform long and cross acceleration, and eotvos – which is used to describe the plane’s velocity with or against the rotation of the earth at a specific latitude – as well as the gravity data, and noted any values or graphs that appeared incorrect. I imported the data from MatLab into a database in Oasis Montaj, and compared profiles of eotvos, ellipsoid height, and the unprocessed data for consistency. Ellipsoid height is used in gravity corrections rather than the geoid, since ellipsoid height is calculated using a shorter wavelength. When checking the magnetic data on MatLab I focused on three to four segments of data from different times during the flight. For each segment I viewed one plot for the Cesium3 magnetometer that included minimum, maximum, mean, and standard deviation, and another for the fluxgate magnetometer with graphs for the fluxgate x, y, z, and sum; the 4<sup>th</sup> differential for the Cesium3 and fluxgate magnetometer were also plotted. In addition, I checked the base station magnetometer data in Oasis Montaj, examining profiles of the raw total magnetic field data and data with a thirty-minute low pass filter applied, reporting deviances in signal quality and any unusual high frequency or amplitude peaks that might signify interferences in the magnetic field or equipment failure.

Both gravimeters use a gimbal to stabilize motion of the platform in three axes: roll, which refers to the longitudinal axis of the plane; pitch, the lateral axis; and yaw, the vertical axis. The gimbal is a fundamental component of airborne and marine

gravimeters, as acceleration of the aircraft will affect gravity values. While the dynamic gravity system (DGS) gravimeter is built for airborne surveys, the zero-length spring (ZLS) gravimeter – which receives its name from the concept that, given that the tension of the spring is proportional to the length of spring, spring length would contract to zero in the absence of external forces (*Lillie, 1999*) –is designed for marine surveys, which means that the accelerometers were not designed to account for intense accelerations that occur on an aircraft, such as taking off, turning sharply to switch lines, or landing. Consequently, the ZLS inflight operating procedure was slightly more complicated. Before take-off, the spring tension was disengaged, the meter clamped, and the torque motors disengaged. Flight line data collection began after acceleration effects were moderated and the aircraft was aligned with the survey grid. To prepare for the first flight line or when approaching a new flight line at a slightly different latitude, we used a spring tension calculator to determine the amount of relative spring tension change. When the flight line data started the torque motors were turned on to engage the platform, and after waiting ~20-30 seconds for the motion to dampen, the meter was unclamped. When stationary, the raw beam's position is zero. After unclamping the meter, however, it is important to check the beam and if it is wildly out of position, slew the beam to zero by pushing a toggle switch. Then, once the total correction settles to fairly small and reasonably stable values, the spring tension is engaged. In heavy cloud cover, pilots will alter the elevation of the plane during the line, called draping. During drapes, the spring tension is disengaged while the torque motors remain functioning to keep the platform stable. The two magnetometers remain in the IcePod after installation for all flights, and are operated by the IcePod Engineer inflight.

### *Data Management and Modeling Software*

Oasis Montaj (GeoSoft ©, [http://pages.geo.wvu.edu/~wilson/gmsys\\_49.pdf](http://pages.geo.wvu.edu/~wilson/gmsys_49.pdf)) software is widely used for management of geophysics datasets within a geospatial framework. The map and grid software allow me to work with new ROSETTA-Ice data layers, as well as legacy datasets (CWA, BEDMAP2, Figure 3). Measured gravity and magnetics data from flight line records can be plotted and viewed as 2D profiles using an Oasis Montaj extension, GM-SYS. Using GM-SYS, it is possible to render 2D crustal transects as geological profiles made up of sectors and polygons that have assigned density and magnetic susceptibility characteristics. By forward modelling, an initial basic model is improved iteratively by inserting polygons with varying densities and susceptibilities ultimately to produce the best calculated fit for the observed geophysical data (e.g., *Monastero et al.*, 2005; *Worthington et al.*, 2016). I have imported grid and point geophysical data from ROSETTA's 2015 survey into a database in Oasis Montaj (GeoSoft ©), together with cover thickness (Figure 6; *Wilner et al.*, 2016) and gravity-inverted bathymetry (Figure 9; *Tinto et al.*, 2016).

The current bathymetry, magnetic and gravity data acquired so far are displayed in Figures 9, 10and 11. Direct flight line measurements of gravity and magnetic data are available along these lines. Further preparation of data for lines 310 and 720 involved sampling the depth to magnetic basement, and bathymetry from interpolated map datasets. Decisions about geology to be depicted in a 2D model entails the close reading of relevant literature to establish a basis for decisions that bear upon the tectonic history, glacial history, bedrock geology, and model parameters, i.e., density and magnetic susceptibility measurements. Geologically reasonable density and magnetic susceptibility

values to use in my Oasis Montaj models are tabulated in Table 1. The Swanson Formation, Ford Granodiorite, Cenozoic volcanics, and migmatites from Edward VII Peninsula and the Alexandra Mountains have moderate to strong gravity signatures, and the volcanics and migmatites from the Alexandra Mountains have strong susceptibilities. Ferrar dolerites of the central TAM and their correlates in other regions have weak gravity signatures and intermediates susceptibilities. Published data are sparse for West Antarctica because few studies have been carried out there (e.g., *Ferraccioli et al.*, 2002), but are ample for the across the Transantarctic Mountains (*Goodge and Finn*, 2010; *Huerta and Harry*, 2004; *Studinger et al.*, 2004). Therefore, I directly measured the susceptibility and density of representative samples from the Ford Ranges provided by Christine Siddoway. I used Colorado College Geology Department equipment, following training by Megan Anderson. Bulk density measurements involved weighing the samples while they were dry, in water, and in air once saturated with water. I used a Kappameter susceptibility bridge to determine the magnetic susceptibility, in  $\text{SI} * 10^{-3}$  units. I measured four different faces for each rock and used the highest value.

## Data

The magnetic anomaly map for the Ross Ice Shelf (Figure 10) comes from a grid based on magnetic data acquired through the 2015-2016 ROSETTA-Ice aerogeophysical survey on flight lines spaced 10 km apart. Values over the whole shelf range from -2400 nT – -2000 nT with blues indicating lower values and pinks higher values. There exists a sharp transition in magnetic anomalies from east to west roughly in the middle of the Shelf; it's trend is north-south. The western half of the Ice Shelf is dominated by negative anomalies while the eastern half is characterized by abundant positive and negative

anomalies. A SW—NE oriented narrow lineament of dark blues in the west roughly aligns with Byrd Glacier, and the lineament is stepped to the left at one point. In the east half of the Shelf, there are NW-SE trending positive anomalies near Siple Coast and further inland. The lateral continuity of the anomaly is not yet known because ROSETTA-Ice coverage currently is incomplete and there is insufficient resolution to image between these anomalies. The gravity anomaly map (Figure 11) is derived from an interpolated grid that also comes from the ROSETTA-Ice survey. A pattern of elongate positive and negative anomalies oriented NW-SE characterize the shelf. Two elongate gravity highs are not entirely continuous, but are separated by areas of lower values. The more southern of these elongate gravity highs is stepped to the west, with somewhat of a ‘hockey-stick’ shape.

The depth to magnetic basement grid (Figure 6 & 12) calculated by *Wilner et al.*, (2016) was imported into both 2D profiles. This critical dataset marks the contact between non-magnetic and magnetic material with well lithified, competent rock. Prospectively, the contact provides a good indication of sediment thickness. A SW-NE trend for highs and lows upon the top of the magnetic basement characterizes western part of the Shelf stretching out from the outlet of Byrd Glacier. The bathymetric high of Roosevelt Island spatially corresponds to an area of shallow depth to magnetic basement. The Depth to Moho modeled (Figure 13) by *Chaput et al.*, (2014) ranges from 18 km – 40 km. The grid shows a concentric shallow region in the middle of the Shelf.

#### *Survey Line 310*

The magnetic data along the line 310 ranges from 2380 – 2040 nT (Figure 14), dominated by long wavelength, low amplitude anomalies. Three positive short

wavelength, small amplitude anomalies appear in the middle of the profile and there is one very short wavelength, high amplitude anomaly in the east. The contact between cover and magnetic material is relatively shallow where the three grouped, positive anomalies. The magnetic high in the east spatially corresponds to a shallow depth to magnetic basement. The gravity data in survey line 310 ranges from -67 mgal to -16 mgal. The anomalies have long wavelengths and moderate amplitudes. The minimum Moho depth is about 21,000 meters at its shallowest and the maximum is about 26,800 meters at its deepest. The depth to magnetic basement reaches almost 5,700 meters, and 1,000 meters at its shallowest.

#### *Survey Line 720 (East)*

The profile displays long wavelength, short amplitude magnetic anomalies, with several short wavelength, moderate to high amplitude anomalies (Figure 15). Gravity values range from -78 to 10.2 mgal. A moderate wavelength, high amplitude positive anomaly occurs over Roosevelt Island. To the west of Roosevelt Island in the Eastern Basin, gravity data display a broad negative low. The Moho depth extends to about 26,500 meters at its deepest and about 20,500 meters at its shallowest. The depth to magnetic basement has a maximum depth of 4,100 meters and a minimum of 1,800 meters.

#### **Modeling**

The layers (horizons) in my GM-SYS profiles of lines 310 and 720, from top to bottom, are the Shelf surface, ice base, and bathymetry acquired by ROSETTA-Ice (*Tinto*

*et al.*, 2016), depth to magnetic basement (*Wilner et al.*, 2016), and depth to Moho (*Chaput et al.*, 2014).

Magnetic field parameters such as magnitude of the total field, inclination, and declination, were inputted into GM-SYS models to account for magnetic field values at the specific locations of the transects. Using the latitude and longitude values for each transect, I used the online geomagnetic calculator provided by the National Oceanic and Atmospheric Administration (NOAA). NOAA's uses the World Magnetic Model, which estimates the rate of change in earth's magnetic field and is recalculated every five years; it was last updated in 2015. The field parameters used for each transect are listed in Table 3.

*Table 3: Magnetic field parameters used for models, calculated using NOAA's world magnetic model (Magnetic Field Calculators, <https://www.ngdc.noaa.gov/geomag-web/#igrfwmm>, April 2017).*

Survey Line	Latitude	Longitude	Total Field (magnitude)	Field Inclination	Field Declination
720 east	78° S	170 ° W	60,950 nT	-78 °	110
720 west	78° S	175° E	61,989 nT	-79 °	130
310	83 ° S	170 W	59,406 nT	-76 °	138

The data-linking function in Oasis Montaj, which allows me to trace a position within the transect simultaneously in the model and in map view, is used to examine the spatial position of features or patterns within the profile versus the map grids. Anomalies with high gradients and/or amplitudes that form continuous linear or curvilinear trends, potentially correspond to faults or tabular, steep, intrusions of mafic rock. Sharp truncations of bathymetric features also indicate the presence of faults. Generally, when attempting to manipulate a body of dense rock to match a steep gravity gradient caused

by some kind of fault, increasing the dip of the body will improve the fit between the calculated and observed curves, and decreasing the dip will improve the fit for a more gradual gravity gradient.

Gravity models use standard density values of  $1028 \text{ kg/m}^3$  for sea water,  $915 \text{ kg/m}^3$  for ice,  $3330 \text{ kg/m}^3$  for the mantle, and  $2670 \text{ kg/m}^3$  for the average continental crust (*Rudnick et al.*, 2003) in the initial models for both survey lines. As a starting condition, I used the depth to magnetic basement layer as a marker for the fundamental contact between a lower region of dense well-lithified “basement” rock, that in its upper extent has some magnetic susceptibility, and “cover” material comprising moderate to low density non-magnetic material that could be sediment.

#### *Survey Line 310 Procedure*

Since the magnitude of magnetic field anomalies strongly differs from east to west, I assigned a lower magnetic susceptibility of  $0.01 \text{ K}$  for the average crust in the western sector bordering the Transantarctic Mountains and a higher value of  $0.025 \text{ K}$  for the eastern half bordering Marie Byrd Land (Figure 16). The transition in susceptibility lies approximately  $230 \text{ km}$  east of the TAM. Low wavelength, moderate amplitude anomalies in the magnetically quiet western sector are resolved by small horizontal shaped polygons with a magnetic susceptibility of  $0.06 \text{ K}$ . To the east there are three short wavelength, high amplitude anomalies, that are reasonable well fit by the transition in susceptibility magnitude. The fit is improved by the introduction of two small tabular bodies with a magnetic susceptibility of  $0.037 \text{ K}$ . The bodies spatially correspond to Crary Ice Rise. Two high amplitude magnetic anomalies over the gravity low to the east are resolved by two tabular bodies reaching greater depths.

A long rectangular sector above the mantle representing a lower crust with higher density produced a more realistically crustal profile. Experiments with different densities for a lower crust yielded a density of  $2800 \text{ kg/m}^3$  that best fits the observed gravity anomaly. The modeled gravity anomaly at the eastern edge of the transect was initially far smaller than the observed, probably due to the downwarped Moho, thicker crust, and thick layer of material above the magnetic basement. To achieve a better fit, I inserted a polygon with a density of  $3000 \text{ kg/m}^3$  and a magnetic susceptibility of 0.046 K. To the west, two tabular bodies introduced to address the high amplitude magnetic anomaly are modeled well with a density of  $2670 \text{ kg/m}^3$ . The paradox of the positive gravity anomaly over the layer of cover was addressed with the introduction of a large polygon directly below the basin with a density of  $2900 \text{ kg/m}^3$ . Small horizontal polygons with densities of  $2500 \text{ kg/m}^3$  helped correct the calculated gravity data for the short wavelength, short amplitude anomalies to the west of Crary Ice Rise. On the western most portion of the transect by the Transantarctic Mountains, the calculated gravity curve arising from the standard lower crust initially fell much lower than the observed data, similar to the Marie Byrd Land side. A large polygon placed at depth with higher densities of  $2900 \text{ kg/m}^3$  and  $3000 \text{ kg/m}^3$  improved the fit in the model. The rock type envisioned for this sector the transect is some kind of mafic intrusion, possibly a gabbro.

In the next iteration of the model 310 (Figure 17), a density gradient at the eastern edge of the transect improved the fit of modeled to observed gravity. The gradient is from  $3100 \text{ kg/m}^3$  on the bottom, decreasing upward through  $2950 \text{ kg/m}^3$ ,  $2850 \text{ kg/m}^3$ , then  $2750 \text{ kg/m}^3$ . The density and magnetic susceptibility of the long tabular body associated with the high amplitude magnetic anomaly to the west were increased to  $2.7 \text{ g/cm}^3$  and

0.05 K. The tabular body adjacent to this was greatly reduced in size but has a stronger magnetic susceptibility of about 0.037 K. A structure having these characteristics could be a vesicular, mafic dike.

The polygon beneath the grounding line on the eastern part of the transect has a density of  $3000 \text{ kg/m}^3$ , appropriate for mafic rock, occurring as a type of mafic intrusion (Figure 17). The tabular body just to the west, attributed with a high magnetic susceptibility and low density, could be a vesicular, igneous body, such as a volcanic rock. To account for the positive gravity anomaly approximately about 362 kilometers from the west end of the transect, a trapezoidal shape has with a density of  $2900 \text{ kg/m}^3$  underlying the layer of cover and is introduced above the elevated portion of the mantle. The high density requires that this body is a mantle-sourced intrusion, probably gabbro. The two small tabular bodies bordering this mafic intrusion modeled to achieve a good fit with narrow magnetic anomalies have a stronger magnetic susceptibility, but are less dense. Based on position, shape, and geophysical characteristics, the rock type depicted by these polygons could be mafic dikes sourced from the gabbro intrusion, possibly exploiting pathways provided by faults.

An alternative approach to modeling profile 310 (Figure 18), I used the GM-SYS inversion tool in a semi-automated fashion. The inversion method allows to specify either density or magnetic susceptibility –holding one parameter fixed to a certain degree – and selecting the standard width polygons for consideration. I divided the lithosphere into large crustal blocks and used this tool to optimize density, which instantly created a decent fit for the gravity. The crustal block furthest to the east, that extends to the end of the profile where there is no data, has density of  $2670 \text{ kg/m}^3$ . The sector of the

lithosphere associated with the group of positive gravity anomalies over the basement low at the eastern edge of the survey line has a higher density of about  $2800 \text{ kg/m}^3$  than the other blocks in the eastern part of the transect. Continuing west, the crust in the rest of the profile is partitioned into three main blocks, with densities of  $2640 \text{ kg/m}^3$ ,  $2680 \text{ kg/m}^3$ , and  $2670 \text{ kg/m}^3$ . Since the magnetic susceptibilities for the average crusts in the previous models were probably far too high, I imposed a reduction in susceptibility for the crust, while retaining the contrast between the east and west portions of the crust. Although the mean error between the modeled and observed magnetic data in this new iteration is only slightly less, the magnetic parameters are more geologically reasonable. Magnetic susceptibility of polygons is more similar or equal to measured values from bedrock of the surrounding region (Table 1 & 2). The dense crustal block in the east has a magnetic susceptibility of  $\sim 0.013 \text{ K}$ , with upper less dense portions with magnetic susceptibilities ranging from  $0.030 \text{ K}$  to  $0.046 \text{ K}$ , while the rest of the crust in the east has a lower average susceptibility of  $\sim 0.000075 \text{ K}$ . To better fit the weaker magnetic signature on the Transantarctic Mountain side of the survey, evident both in the magnetic data in the profile and clearly in mapview, weaker susceptibilities of  $0.00001 \text{ K}$  were assigned. Also, a non-magnetic lower crust is introduced. The horizontal green line in this region of the profile separates the crust into an upper magnetic portion and a lower non-magnetic portion. The concept is that there is an elevated Curie isotherm, as a consequence of the elevated temperature is in the crust where the Moho is shallow (*Ferraccioli et al., 2001; Lillie, 1999*). The Curie depth is at 14,000 meters on the west side and about 19,800 on the east side.

In this iteration (Figure 18), the dense polygon in the west side of the transect was moved further at depth to better fit the positive gravity anomaly coupled with low frequency magnetic data. The shape of the polygon was changed to incorporate denser layers of upwelled mantle and lower crust, to depict crustal necking (*Beek et al.*, 1994; *Huerta and Harry*, 2004) and achieve a closer match between the calculated and observed curves. Density values of  $3000 \text{ kg/m}^3$  for the lower crust and  $2900 \text{ kg/m}^3$  for the rest of the body were assigned. To improve the fit, the depth to Moho layer calculated by *Chaput et al.*, (2014) was altered. Grounds for the change come from evaluation of proximal Ross Sea flight lines acquired by NASA IceBridge (unpublished, Kirsty Tinto and Christine Siddoway). The tabular polygon in the east side attributed with characteristics of a vesicular, volcanic neck, fits the observed data, namely the short frequency, high amplitude magnetic anomaly and negative gravity anomaly. The polygon was widened and assigned a magnetic susceptibility of  $0.021 \text{ K}$ . Upper blocks have susceptibilities of  $0.038 \text{ K}$  and  $0.024 \text{ K}$ . The higher nT values in the magnetic data to the east are better fit with the bottom surface of the polygon dipping to the east, rather than being horizontal. The tabular shapes, located at the margin of the basin west of the dense polygon, have magnetic susceptibilities of  $0.020 \text{ K}$  to  $0.045 \text{ K}$  to address the three short frequency, moderate amplitude anomalies associated with Crary Ice Rise.

For all iterations of line 310, the magnetic data throughout the entire profile was better fit with a susceptibility of  $0 \text{ K}$  assigned to the layer above the magnetic basement horizon, separating the crustal blocks. Initially, with a standard crustal density ( $2670 \text{ kg/m}^3$ ) assigned to the entire upper crust (*Rudnick et al.*, 2003), together with a higher density lower crust ( $3000 \text{ kg/m}^3$  –  $3100 \text{ kg/m}^3$ ) and mantle ( $3300 \text{ kg/m}^3$ ), the calculated

gravity anomalies within the whole transect were far greater in magnitude than the observed anomalies. The gravity data throughout the profile was improved by modeling the layer above the magnetic basement horizon with a weaker density of  $2400 \text{ kg/m}^3$ . Based on these geophysical properties and the significance of the position of the magnetic basement contact with respect to this layer and the surrounding crust (*Wilner et al.*, 2016), this cover layer is interpreted to be sediment.

#### *Survey Line 720 (East) Procedure*

Since line 720 extends more than 600 kilometers in length and spans a dramatic shift in geophysical and bathymetric trends seen in map view and in the profile midway across the shelf, I decided to analyze the model in two segments. I clipped the full transect into one new line for the east sector and another for the west sector, extending the margins of each. For the eastern part of line 720, my modeling approach involved use of the GM-SYS inversion tool at the outset (Figure 19). The output was the geometry of the polygons in the subsurface that fit the measured gravity anomalies. The gravity data for the central Ross Sea have long positive wavelengths that can be fit with rectangular polygons having a density of  $2500 \text{ kg/m}^3$  directly under the shallow magnetic basement contact. To the east, there is a negative long wavelength anomaly that corresponds to an increased layer of cover. A large polygon with a density of  $2600 \text{ kg/m}^3$  aligned with this anomaly helped match the calculated and observed gravity data fairly well. A long, thin horizontal body with a density of  $3000 \text{ kg/m}^3$  west of and beneath Roosevelt Island produced a good fit between the calculated and the observed curves. In the first iteration, this dense sector was modelled using magnetic susceptibilities ranging from  $0.015 \text{ K} - 0.047 \text{ K}$ . These variations in magnetization within the same body helped fit the magnetic

signature on the east portion of the transect. The large polygon with a density of 2600 kg/m<sup>3</sup> on the eastern side of Roosevelt Island was assigned a susceptibility ranging from 0.035 K – 0.045 K. The high amplitude anomaly present in both potential fields data over Roosevelt Island is produced by an elevated portion of the 2600 kg/m<sup>3</sup> and 3000 kg/m<sup>3</sup> bodies.

The next iteration of the profile (Figure 20) was also modeled using the inversion tool, but this time beginning the forwarding model process first by constraining the gravity data by the dividing the crust into blocks, as in line 310. Large crustal sectors with an average density of 2700 kg/m<sup>3</sup> achieved a good fit between the calculated and observed gravity data. To address the high amplitude anomaly associated with Roosevelt Island, the depth to magnetic basement horizon was altered to incorporate a section of upthrown basement rock, in keeping with the previous interpretation of *Wilson and Luyendyk, 2006* (Figure 21).

Decision about modeling of 720-east of magnetic data profiles were informed by the outcomes of line 310 modeling. Susceptibility values were used that are more geologically reasonable, i.e., they are more consistent with known values of the surrounding geology (Table 1 & 2), for granitoids and metaturbidites that make up the upper crust of Marie Byrd Land (*Ferraccioli et al., 2002; Luyendyk et al., 2003*). The crustal block on the western edge of the profile, where there is no data, that extends towards the middle of the Shelf, has a magnetic susceptibility of 0.00001 K; this value is consistent with the susceptibility used for the crust in the western half of model 310 (Figure 20). The crustal block on the west edge of transect, where data in the profile begins, has a higher magnetic susceptibility of 0.000075 K, and the rest of the crust

required stronger values around 0.020 K to bring the calculated curve closer to the observed data. The rock type for these crustal blocks is likely a granitoid. The larger, magnetized polygons in the last iteration of the model were replaced with several small polygons of intermediate to high magnetic susceptibility placed the top of the magnetic basement contact, to correct for the magnetic anomalies. Small rectangular units with magnetic susceptibilities over 0.03 K to 0.05 K were required to fit the moderate amplitude magnetic anomalies over the Eastern Basin, but densities remain similar to the surrounding crust. The negative anomaly east of Roosevelt Island, covering Roosevelt Sub-basin (*Sorlien et al.*, 2007) is fairly well fit by the non-magnetic layer of cover and a small polygon at magnetic basement horizon with a weaker susceptibility of (about 0.012 K) than that of the host rocks. Further east, rectangular polygons with susceptibilities ranging from 0.030 K to 0.035 K reduce the misfit between the calculated and observed data over the moderate amplitude, short and moderate frequency anomalies. The rock type for these smaller polygons at the magnetic basement contact are interpreted to be low to medium grade metaturbidites. The short frequency, high amplitude magnetic anomaly over Roosevelt Island in this model is better fit by a thin dense tabular shape with a susceptibility of 0.056 K. The rock type for this tabular polygon is interpreted to be a mafic body.

Similar to model 310, magnetic data within initial profiles for survey line 720-east produced using a susceptibility of 0 K for the cover layer best fit the observed magnetic data. A density of  $2400 \text{ kg/m}^3$  for this material also improved the fit between the calculated and observed gravity data in all areas. Based on the strong density contrast between the non-magnetic layer and the underlying magnetic crust, separated by the

depth to magnetic basement horizon (*Wilner et al.*, 2016), the rock type interpreted for this material is sediment.

## **Discussion**

### *Geophysical Modeling*

The geometry of polygons and lateral density variations within model 310 indicate contrasts in bedrock lithology that align with steep gradients in the magnetic and gravity data (Figure 18). These characteristics are interpreted to be the result of normal faulting, in keeping with the known tectonic history of the region (*Siddoway*, 2008, 2016).

The Ross Embayment underwent large-scale continental rifting in the Cretaceous, thinning the crust and raising the Moho depth. Therefore, normal faults interpreted in the model are reasonable since they are common in extensional settings of continental crust. A study by *Muto et al* (2013) hypothesized that a fault exists at the base of Whillans Ice Stream, and continues to the margin of Crary Ice Rise. Based on the gravity data at the station near Whillans Ice Stream (Figure 22), the upthrown portion of basement rock is on the east/southeast. The fault proposed by *Muto et al.*, (Fig. 2013) extends linearly over hundreds of kilometers (Figure 21); this is not physically realistic. Two normal faults – rather than one – dipping east and west (in profile, not mapview) are responsible for the bedrock high, and the gravity gradients from north to south can be attributed to the density contrasts of the upthrown basement rock. The mafic intrusion in my model to the east of CIR, which lies directly under the basement low and is bounded by steep faults, accounts for the positive gravity anomaly. Faulting may provide conduits for mafic magmas. Therefore, the small tabular bodies west of the mafic intrusion that resolve the

positive magnetic anomalies are plausible. These polygons are interpreted to be mafic dikes, which may provide sources of heat to ocean water or grounded ice above. Near the Transantarctic Mountains – Ross Ice Shelf boundary, crustal necking is depicted to resolve the high magnitude gravity anomaly (Figure 18). Models of mantle and crustal necking at the TAM- Ross Sea boundary have been proposed by Crustal necking produced during rifting at the margin between the TAM and the Ross Sea likely also may have occurred along the Ross Ice Shelf-TAM boundary.

The modeled profile of survey line 310 displays a positive gravity anomaly over the layer of cover and a pronounced magnetic anomaly at the basement low margin over the bathymetric high (Figure 18). The contacts between the more magnetic body with the dense crustal block and the surrounding crust roughly align with the steep gradients in the magnetic and gravity data. This polygon could reflect a body of rock that was affected in a zone of shearing and highly magnetized. The relief upon the magnetic basement and the contrast in bedrock lithology suggest that the basement high and geophysical signatures are structurally controlled. East of these structures is Siple Dome, a prominent bedrock high that diverts the flow of major ice streams from the West Antarctic Ice Sheet. Previous 2D profiles of Siple Dome have been modeled with high-density, basement rock (Figure 22; *Wilson and Luyendyk, 2006*), and show that this crystalline rock must extend to the edges of the plateau. This suggests that the bathymetric high of Siple Dome is also somehow structurally controlled, rather than a product of sediment accumulation.

Roosevelt Island is a bathymetric high between Roosevelt Sub-basin and the Eastern Basin that exhibits a high amplitude, positive anomaly in survey line 720 (Figure 20). The linear, laterally continuous anomaly, the density contrasts on either side, and the

bathymetric relief suggest that Roosevelt Island is a block of upthrown crust bordering a fault. A fault on the Roosevelt Sub-basin side dips east. Gravity data from previous on-ice surveys have been used to model 2D profiles of Roosevelt Island (e.g., *Wilson and Luyendyk*, 2006, Figure 21), with an elevated portion of basement rock and small packages of low-density sediment in troughs. The profile from *Wilson and Luyendyk* (2006) is modeled using free air gravity anomalies, only extends to a depth of one and half kilometers, and uses a density value of  $2000 \text{ kg/m}^3$  for the sediment layer. The depth to magnetic basement horizon in my model, at 2,700 meters depth, provides greater detail for the contact between basement rock and less dense sediment beneath Roosevelt Island. My model verifies that the bedrock beneath RI must not be uniform in order to match the gravity data, but contain both lower density sediment and higher density crystalline rock. By considering magnetic anomalies, the model also enhances knowledge of the rock composing Roosevelt Island, and reveals the possible existence of a mafic intrusion beneath Roosevelt Island. The thin body at the magnetic basement contact is likely some kind of mafic intrusion, based on the high values of geophysical parameters.

#### *Confidence of Constraints from Modeling*

The gravity data in both profiles are well constrained, with a mean error of about 5 mgals. My final models include a sediment layer with a uniform density of  $2400 \text{ kg/m}^3$ . However, there is probably some variation in density, depending on the sediment composition, degree of lithification, and given that sedimentary basins may exhibit stratigraphic sequences following repeated glacial cycles (e.g., in Ross Sea troughs, *Sorlien et al.*, 2007). Future models might include a more detailed interpretation of the

sediment layers, that would be extremely valuable for studying ocean circulation or ice flow above bedrock.

The mean error for the magnetics data in both models is about 24 nTs; further work in GM-SYS is needed to produce a better fit for the magnetic data for both models. In survey line 310, the calculated magnetic anomalies in the entire west side of the transect should be lower to match the observed anomalies (Figure 18). Raising the curie depth or lowering the depth to magnetic basement in this region might obtain a closer fit. The modeled calculated magnetic anomalies roughly fit the three short frequency, positive anomalies by Crary Ice Rise. However, the long wavelength anomaly starting over the mafic intrusion and continuing east is not well fit. To address this, higher susceptibilities should be assigned to subdomains in the subsurface, bringing the calculated data closer to the observed data. The short frequency, high amplitude anomaly in the east needs to be further addressed. The anomaly produced at the base of the steep gradient is still lower than the observed data, and the calculated curve fitting the steep gradient going east is also still below the observed data. In survey line 720, although the gravity data are fit well, all of the magnetic anomalies, particularly the one over Roosevelt Island and those over the Eastern Basin, are poorly fit (Figure 20). In the west part of the eastern line 720, the model produces two magnetic anomalies that have moderate wavelengths and amplitudes, that are not in the observed data. To achieve a fit with the observed data, the modeled anomalies should have broader wavelengths and amplitudes.

The curie isotherm might be more carefully applied to the east half of the transect in line 310. This model depicts the isotherm travelling down in a perfectly vertical line, and then instantly leveling out towards the east for the rest of the transect. Thus, the boundary

between the crust of the western portion (Transantarctic Mountain-type lithosphere) and the crust of the eastern portion (Marie Byrd Land-type crust) is marked by the position of the inferred Curie isotherm. Since West Antarctica is underlain by hot, low viscosity mantle, the Curie isotherm in the eastern portion of my profiles is also likely to be elevated. The Moho layer used in used in my models may also be inaccurate, especially for flight line 720, which has impacts for the shape of the lower and upper crust. The depth to Moho grid in future models should be calculated differently or used primarily as baseline from where it could be altered based on decisions about how to better improve the fit for the gravity data.

#### *Regional Implications*

It is widely accepted that the Transantarctic Mountains mark the lithospheric boundary between the East Antarctic craton and the hot West Antarctic crust. However, recently acquired geophysical data covering the Ross Ice Shelf the and 2D profiles of ROSETTA-Ice lines 310 and 720 reveal that the boundary instead lies midway across the shelf (about 228 kms from the west end of 310, Figure 18) in bathymetric and geophysical trends. The eastern half of the Ross Ice Shelf has pronounced gravity and magnetic anomalies while the western half is magnetically quiet. Different average magnetic susceptibilities apply to the east and west portions of the crust. This profile appears to fall upon the demarcation between the magnetically weak East Antarctic crust and the high frequency West Antarctic crust. The values for magnetic susceptibility used to address the small amplitude, high frequency magnetic anomalies in the west portion of transect 310 (Figure 20, green and orange units) are consistent with values recorded from rock exposures in the central Transantarctic Mountains, including a succession of

Neoproterozoic rift margin sediments and igneous rocks known as the Beardmore Group and Ferrar Dolerite Suite (*Goodge and Finn*, 2010) The central TAM region of the East Antarctic crust was affected by Neoproterozoic and Ross Orogenies. The Ferrar Dolerites have low to intermediate magnetic susceptibilities and in other gravity models (e.g., Figure 8 from *Goodge and Finn*, 2010) produce magnetically noisy, positive anomalies, similar to those in line 310. These Neoproterozoic sediments overly dense, Precambrian basement rock that comprise the bulk of the TAM crust. Within the western portion of profile 310, the upper crust is basically modeled as one dense sector, with a couple other small polygons, interpreted as fairly magnetic sediment. (Figure 18). The geology of the subsurface modeled shares geophysical characteristics with the geology of the central Transantarctic Mountains. If the sediment modeled at the west end of the section is interpreted as sediment from the TAM, then in future models, the less dense, yellow layer should be thinner and the denser, pink crustal block should be thicker. Based on the geologic and geophysical information from the central Transantarctic Mountains region and the fit achieved between the calculated and observed magnetic data in my models, the lithosphere of East Antarctica may extend farther inland into the Ross Ice Shelf than currently believed (Figure 23).

The geology of West Antarctica including Marie Byrd Land, King Edward VII Peninsula, and the Ford Ranges is well known from outcrops and geophysical surveys (*Ferraccioli et al.*, 2002, 2002; *Luyendyk et al.*, 2003; *Wilson and Luyendyk*, 2006) and may continue beneath the Ross Ice Shelf (*Elkind et al.*, 2016; *Siddoway et al.*, 2004, 2016; *Siddoway*, 2008). The western Marie Byrd Land crust consists primarily of metasediments, various granites, mafic dikes, and metamorphic core complexes, in

addition to basalt flows and other volcanics as young as the Pleistocene (*Elkind et al.*, 2016; *Siddoway et al.*, 2016). The presence of numerous igneous centers in western MBL have also been proposed on the basis of geophysical data, acquired in the CWA survey (*Behrendt et al.*, 2007, 2013). Polygons accounting for various gravity and magnetic anomalies within models 310 and 720-east, interpreted to be volcanic necks, mafic intrusions and dikes, that are associated with faulting based on geophysical characteristics and the regional geology, may be related to mafic rocks in western MBL. The location of these faults and mafic dikes, in particular, near the grounding line by Crary Ice Rise (Figure 18), has bearing on ice stream flow and may be sources of elevated geothermal heat (*Fisher et al.*, 2015) that affect Shelf stability.

Previous surveys have also illuminated the tectonic/structural evolution and geology of basins in the Ross Sea (*Beek et al.*, 1994; *Decessari et al.*, 2007; *Karner et al.*, 2005) and sedimentary sequences were imaged by seismic reflection in the Eastern Basin and Roosevelt Sub-basin in a marine survey (Figure 5, *Sorlien et al.*, 2007). Moderate magnitude gravity anomalies over the Roosevelt Sub-basin where there is thick sediment within model 720-east are resolved with high density polygons, and are interpreted to be mafic intrusions. This modeling approach follows that of models by *Karner et al.*, (2005) for troughs in the Ross Sea. My model shows that the geology of the crust beneath the Ross Ice Shelf along extensional basins requires high density, mafic intrusions, similar to the rock beneath the high gravity anomaly rift basins in the Ross Sea. Thick layer of low-density sediment at the eastern edge of 310 interpreted in my models may be related to sediments in western Marie Byrd Land, identified in the subglacial geologic map by *Elkind et al.*, (2016).

Structural features such as faults are identified in my models near the Crary Ice Rise, Siple Dome, and Roosevelt Island (Figure 18, 20) and in structural profile (*Siddoway et al.*, 2016) across the Shelf into western Marie Byrd Land (Figure 23). These portions of the Shelf are all elevated, likely due to vertical displacement during faulting. Basement lows are overlain by thick low-density material, most likely sediment, with volcanic necks or dike systems beneath (Figure 23). The Central High is an elevated, elongate portion of the Ross Sea bathymetry (Figure 4). Map interpolations of the Ross Ice Shelf and Ross Sea calculated by *Wilner et al.*, (2016) show that the Central High extends from the Ross Sea and continues beneath the Ross Ice Shelf to Crary Ice Rise, and then is cut by faults to the south (Figure 6). Based on my model of line 310, the structural transect adapted from *Siddoway et al.*, (2016) should be modified to depict two normal faults dipping east and west mid-Shelf by the Central High, rather than only one fault. The southern continuation of the Central High downstream of West Antarctic ice streams has major consequences for ice flow and ocean circulation. The Transantarctic Mountain-type crust is depicted in the RIS structural transect with uniform geology, thinning east (Figure 23). To improve upon this profile, the crust at the rift boundary should be developed to include different rock types that reflect past extensional processes, and the contact between the two types of crust should be altered based on the contact shown in model 310 (Figure 18).

Patterns in the depth to magnetic basement layer greatly differ between the two transects. The sediment-basement contact in profile 310 fluctuates considerably and has much more topographic relief than in the east or west portion of line 720 (Figures 18 & 20). The magnetic basement in line 310 reaches depths as deep as 5,700 meters and as

shallow as 1,000 meters, whereas in 720 the depth to basement only reaches 4,100 meters maximum and 1,800 meters at its shallowest contact. The contrast in the sediment-basement contact layer and the variations in sediment thickness of the basins could be related to the kind of ocean circulation above the rock. The greater the relief of sedimentary basins, the stronger the temperature, salinity and density gradients. These strong gradients will impact ocean circulation and consequentially influence basal melt and ice shelf stability.

## Conclusion

Transects along flight lines 310 and 720-east were selected for modeling of the geology of the crust beneath the Ross Ice Shelf, using gravity and magnetic data acquired from the 2015-2016 aerogeophysical survey by ROSETTA-Ice. Line 310 begins just inland of the Transantarctic Mountains, passing the grounding line several times through a portion of Crary Ice Rise, and ends near Siple Dome. Line 720, in the northern Shelf, also extends from the TAM, passing through several crustal troughs and along the tip of Roosevelt Island. Models of line 310 and 720-east include geological elements such as mafic intrusions and dikes, crustal necks, sedimentary troughs, and fault systems. Primary rock types interpreted based on geophysical characteristics include metasediments, various granites, gabbro or other mafic rocks, and low-density sediment. Both profiles reveal thin crust, generally consistent with the model by *Chaput et al.*, (2014). However in some places, for instance, the crustal necking in the west side of line 310, the Moho depth must differ from the Chaput model. Interpretations of the bedrock geology are valuable as they identify the location of faults and inferred mafic bodies which may be sources of elevated geothermal heat that influence melting of the Shelf.

These geological elements reflect the fundamental effects of rift processes in the development of the sub-Ross Ice Shelf lithosphere. Aerogeophysical data and models of Ross Ice Shelf transects reveal that the lithospheric boundary between the East Antarctic craton and the West Antarctic crust may extend further inland of the Transantarctic Mountains than currently believed.

## Figures

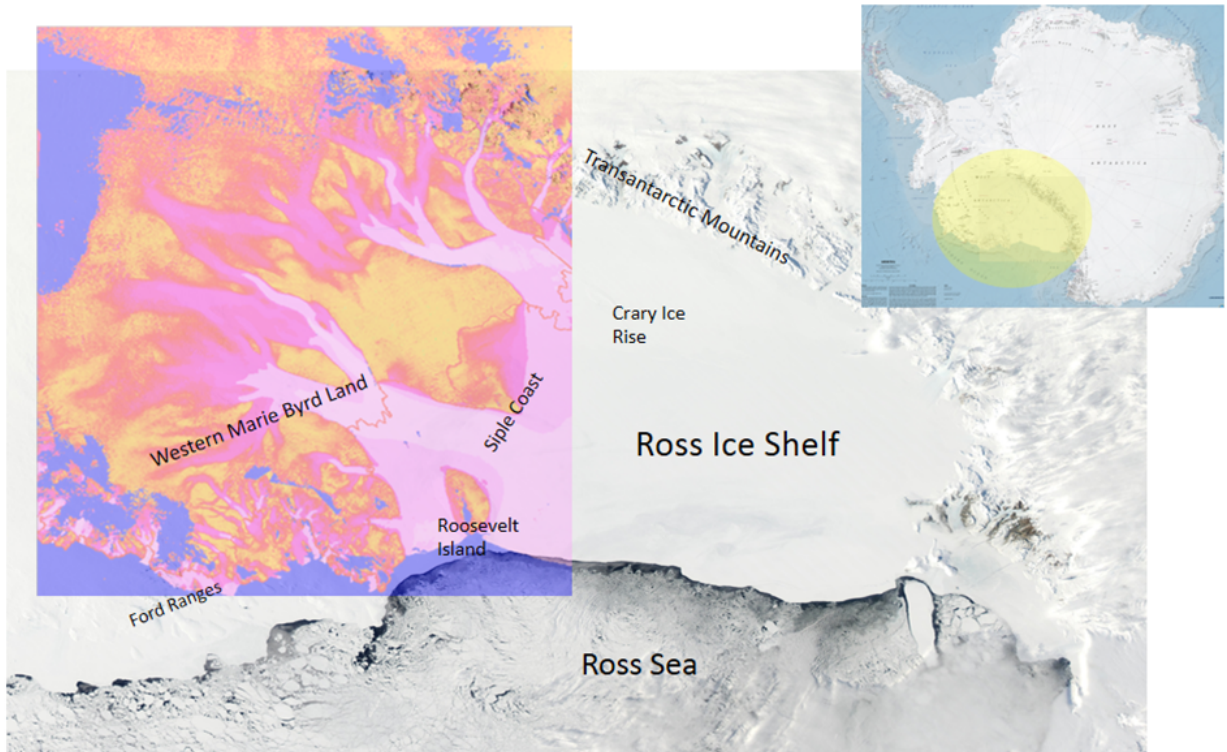


*Figure 1: Map of West Antarctica including the Ross Ice Shelf, Ross Sea, the Transantarctic Mountains, and western Marie Byrd Land. This map comes from MODIS imagery. The inset in the upper right shows this region with respect to the continent; location map is from the Polar Geospatial Center. The map overlain in Marie Byrd Land and the Ross Ice Shelf is a velocity grid for ice flow for the West Antarctic Ice Sheets. Pinks indicate fast velocities (1,000 m/yr) and blues and oranges indicates slower (0 m/yr) velocities. The ice velocity grid was calculated using a model by Rignot et al., 2014.*

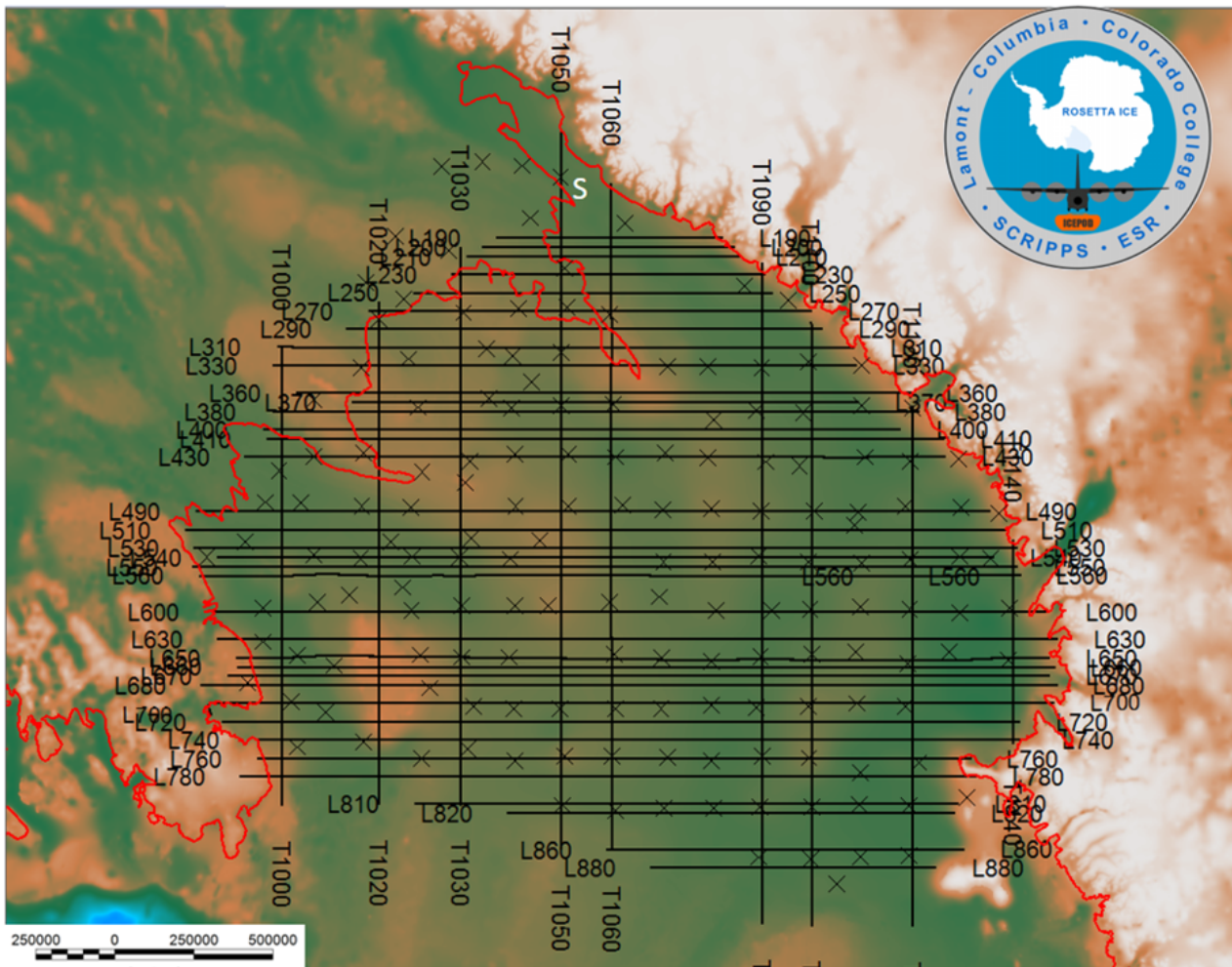


Figure 2: Xs are stations spaced in a 55km grid from the Ross Ice Shelf Geophysical Glaciological Survey (RIGGS), completed in the 1970's. The black grid are the current survey lines flown by the ROSETTA-Ice survey. The numbers correspond to survey flights. The map is BEDMAP2; pinks are bathymetric highs and greens are lows. The red line is the grounding line. The survey lines used in my geophysical models are 310 and 720.

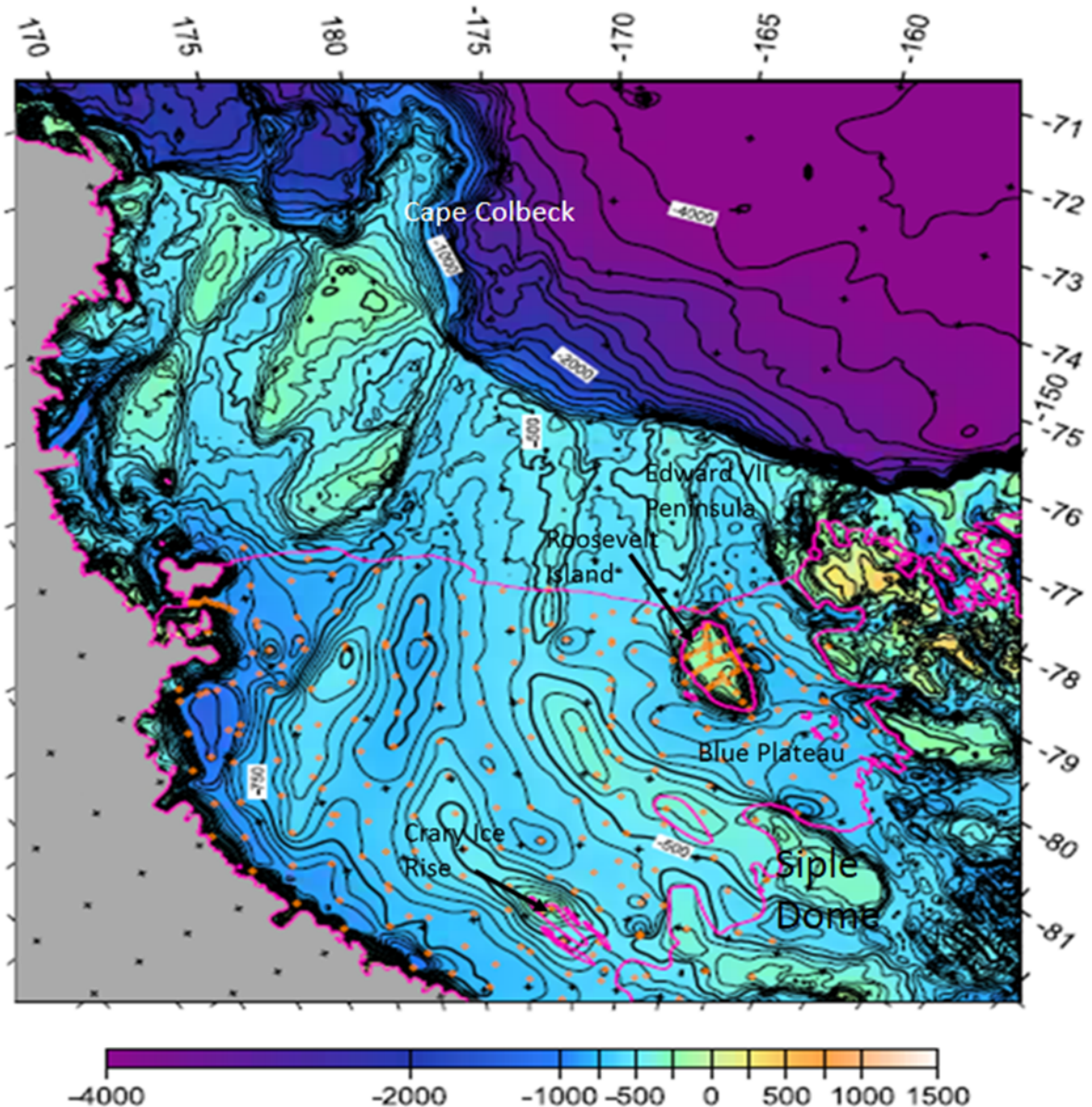


Figure 3: Map of the bathymetry and bed topography for the Ross Sea and Ross Ice Shelf. Data is derived from BEDMAP, Behrendt et al., 2004; Luyendyk et al., 2002; Luyendyk et al., 2003. The pink line indicates the grounding line, and the orange circles represent RIGGS stations. Figure comes from Wilson and Luyendyk, 2006.

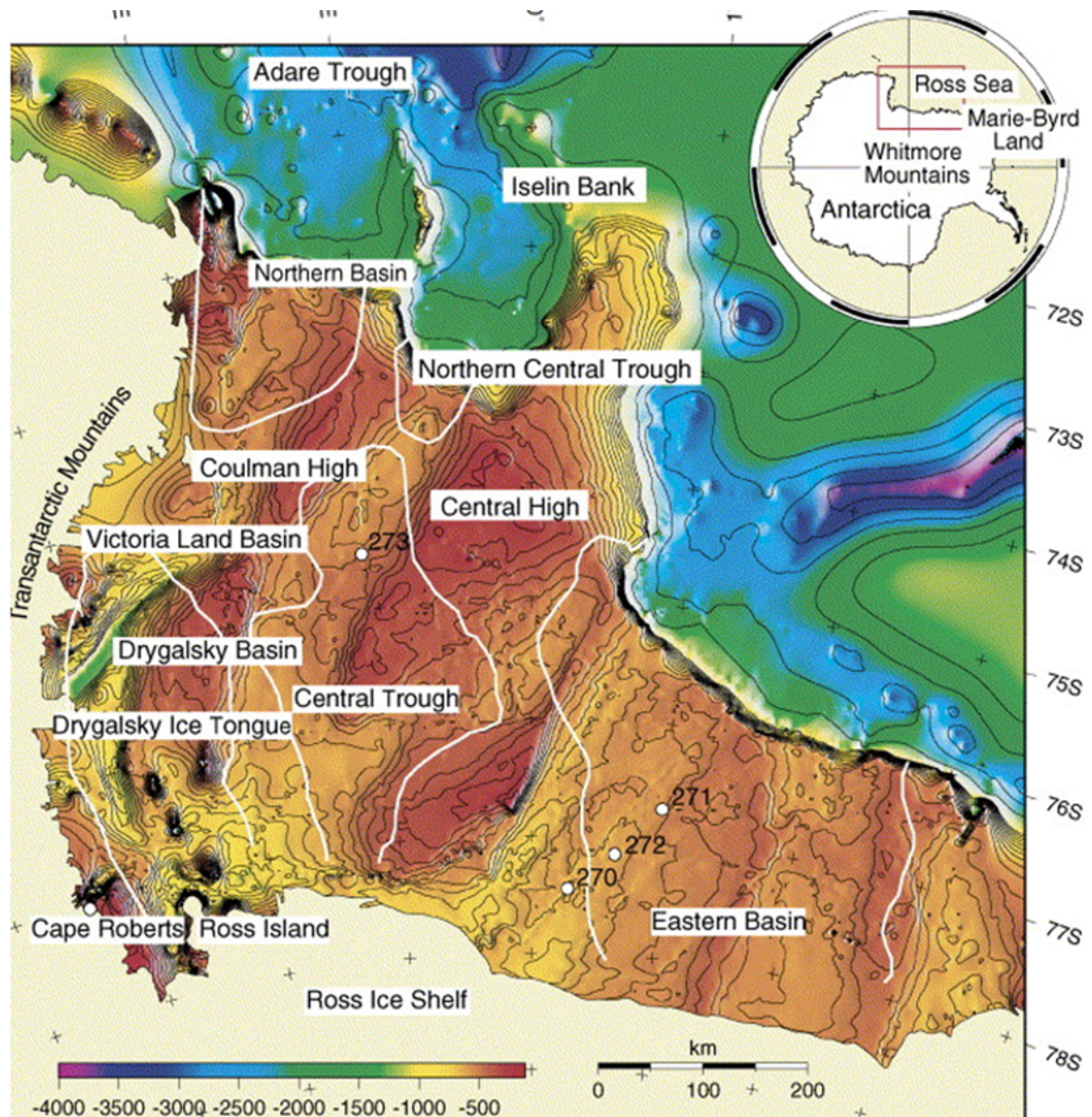
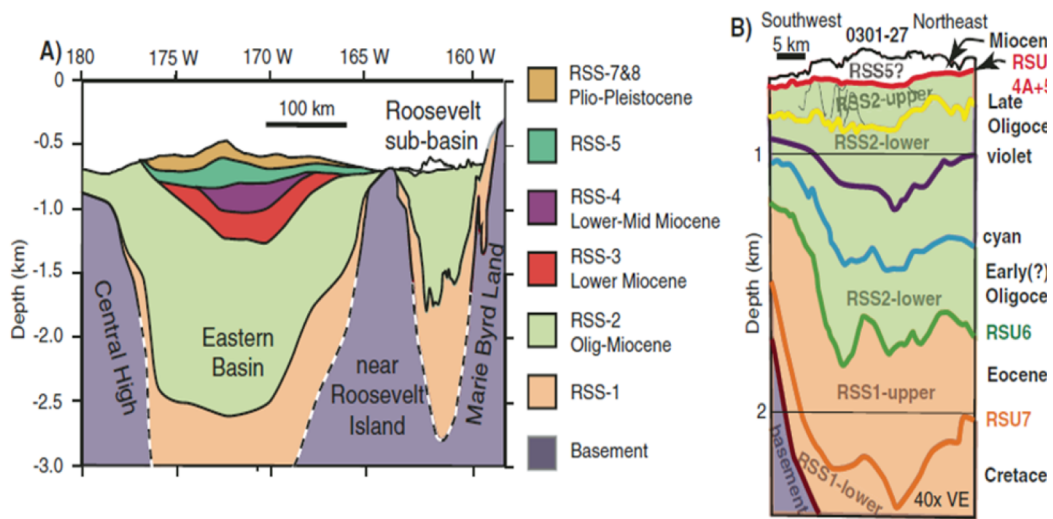


Figure 4: Bathymetry map of the Ross Sea showing crustal highs and troughs. Reds indicate bathymetric highs and greens bathymetric lows. The dark black line marks the ice shelf edge. Image from Karner et al., 2005.



*Figure 5: Cross sections are interpreted from seismic-reflection profiles. A) A cross section in the eastern Ross Sea near the shelf edge covering the Central High, Eastern Basin, the area south of Roosevelt Island, and Roosevelt sub-basin. B) A detailed cross section over Roosevelt sub-basin including units for Ross Sea strata. Figure comes from Sorlien et al., 2007.*

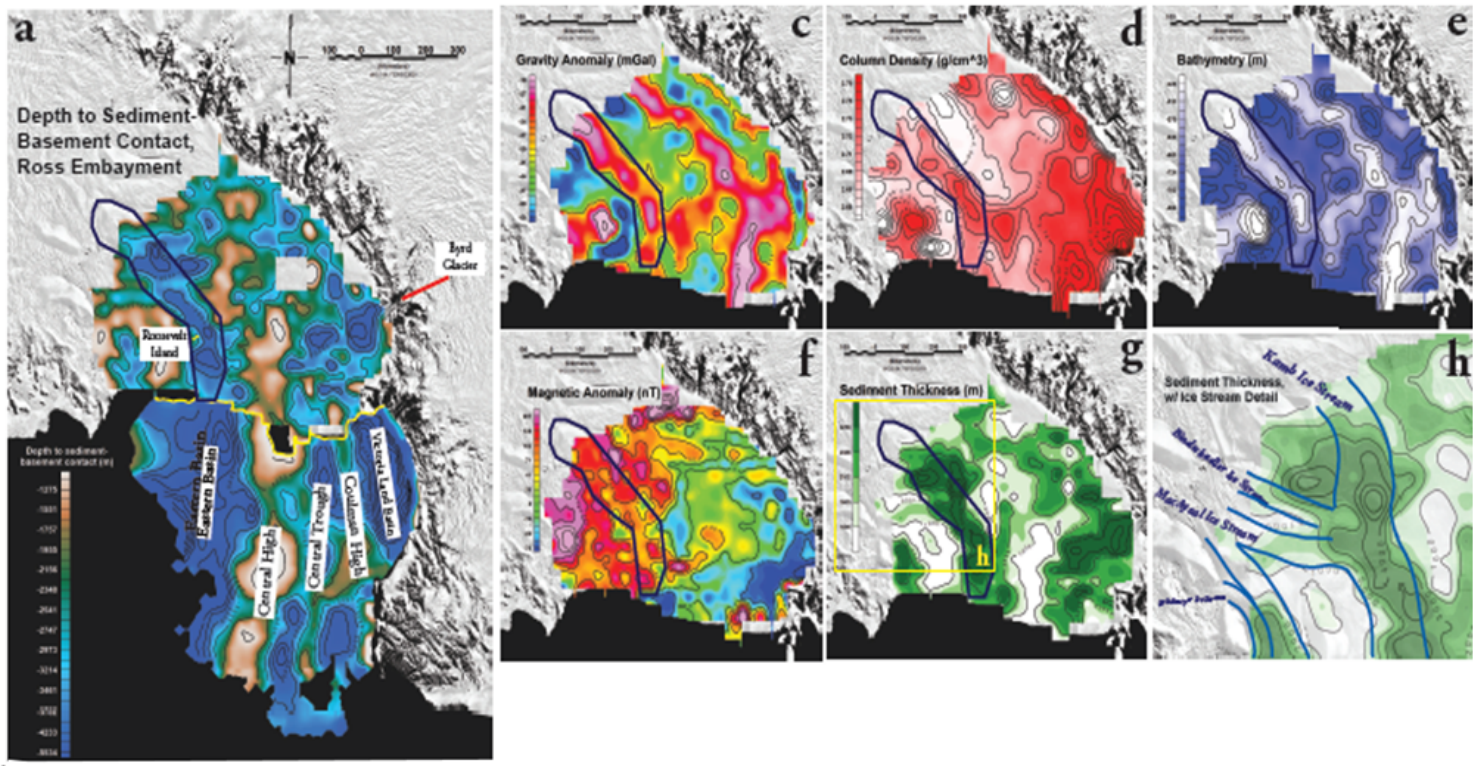
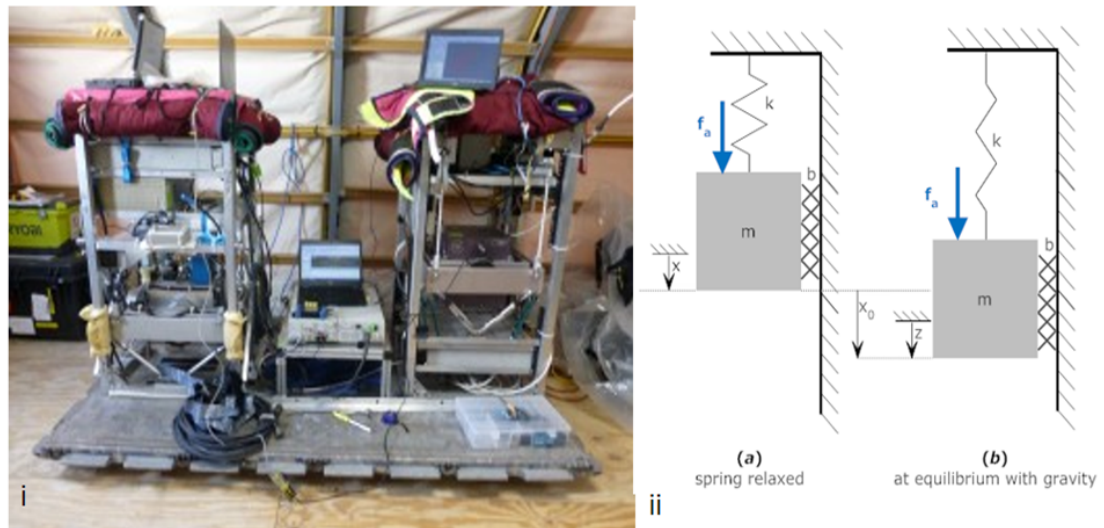


Figure 6: A) Depth to magnetic basement map calculated using Werner deconvolution. Blues indicate deep sediment–basement contacts, and pinks indicated shallow contacts. Columnar density and sediment thickness grids are shown in d) and g). Maps come from AGU poster by Wilner et al., 2016.



*Figure 7: i) Gravimeters used in ROSETTA-Ice's 2016-2017 survey from the left: ZLS, iMar, and the DGS. ii) Basic schematic showing how gravity meters work. They contain a mass connected to a spring and a beam, and as the earth's field changes, the forces exerted on the spring by the mass varies. This changes the position of the mass and the length of the spring; the change in spring length reflects the change in gravity. Diagram taken from <http://lpsa.swarthmore.edu/Systems/MechTranslating/TransMechSysModel.html>.*



Figure 8: Images showing IcePod designed by ROSETTA-Ice, with and without the external panel, attached to a lever arm of an LC-130 aircraft. Nicholas Freason, pod engineer at Lamont Doherty Earth Observatory, checks that the pod is secure.

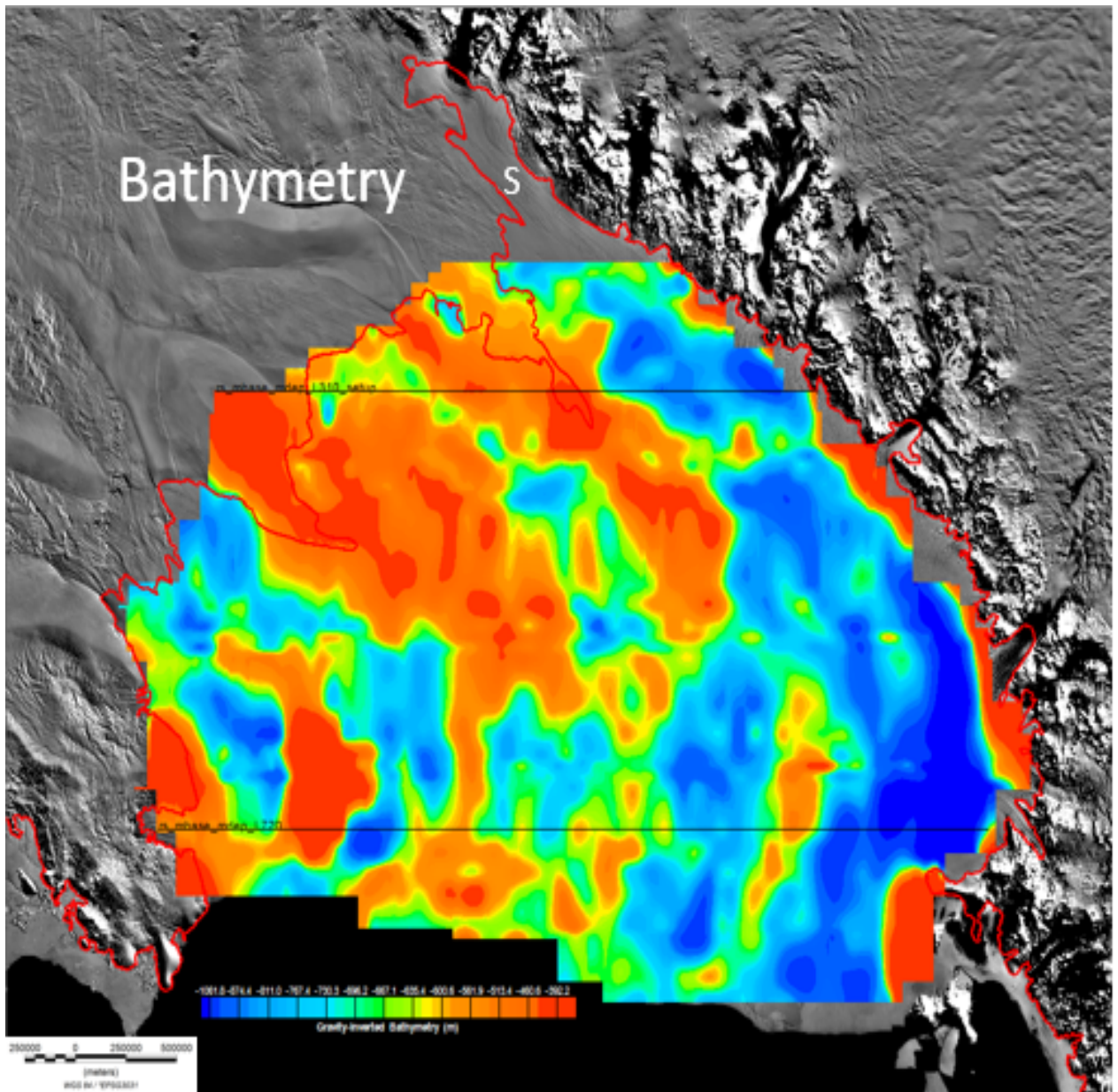


Figure 9: Map of gravity inverted bathymetry beneath the Ross Ice Shelf, calculated by ROSETTA-Ice and overlain on MODIS imagery. The Ross Embayment was subject to extreme extension in the late Cretaceous which is reflected in the basin-and-range style features seen in mapview. Black lines are flight lines and transects used for geophysical modeling.

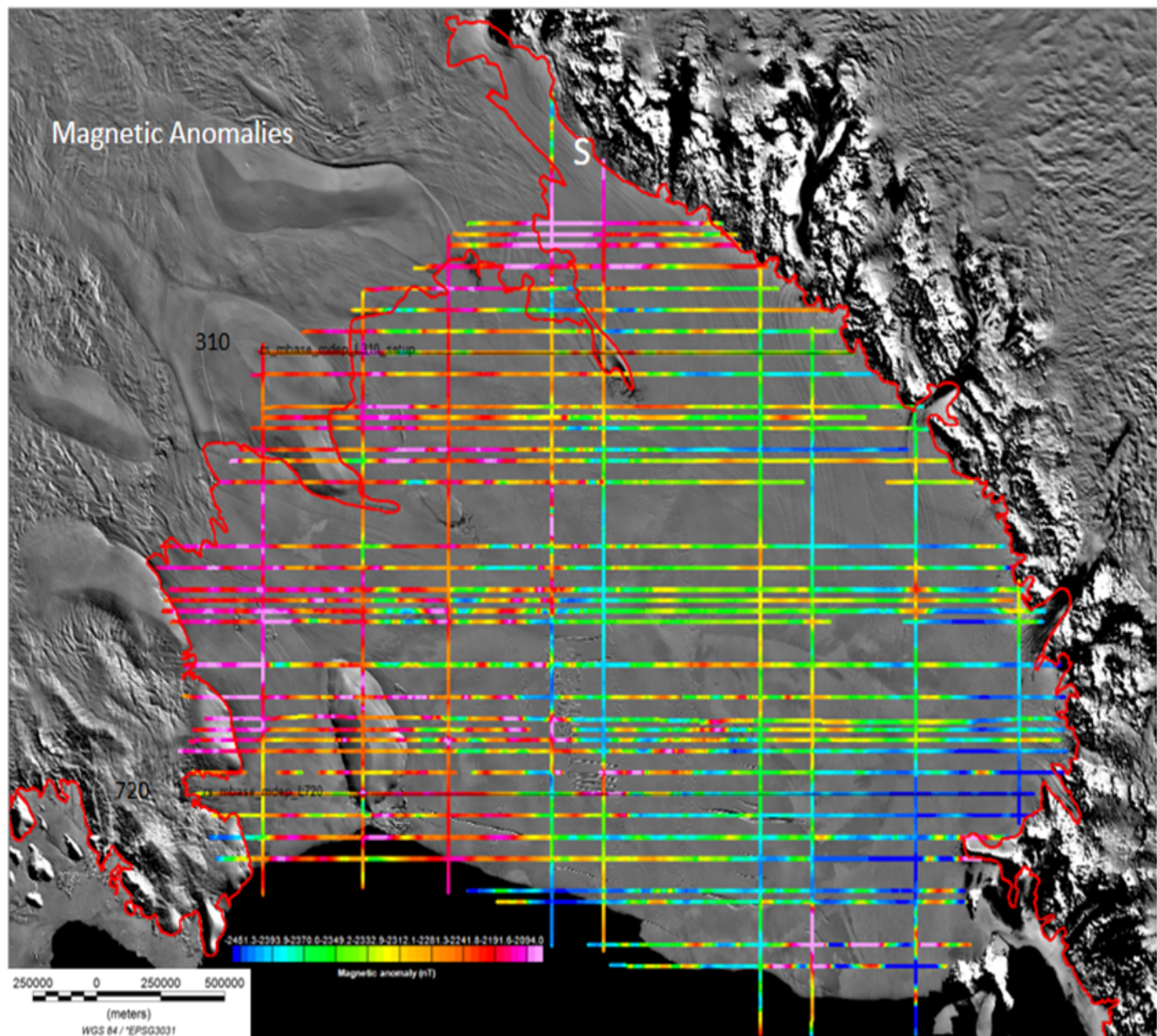


Figure 10: Map of magnetic anomalies over MODIS imagery, with data acquired from ROSETTA-Ice's 2015-2016 aerogeophysical survey. Blues indicate low values and pinks indicate high  $nT$  values; values range from -2450 nT to -2094 nT. The western half of the shelf generally is much quieter magnetically than the eastern half of the shelf. Black lines are flight lines and transects used for geophysical modeling.

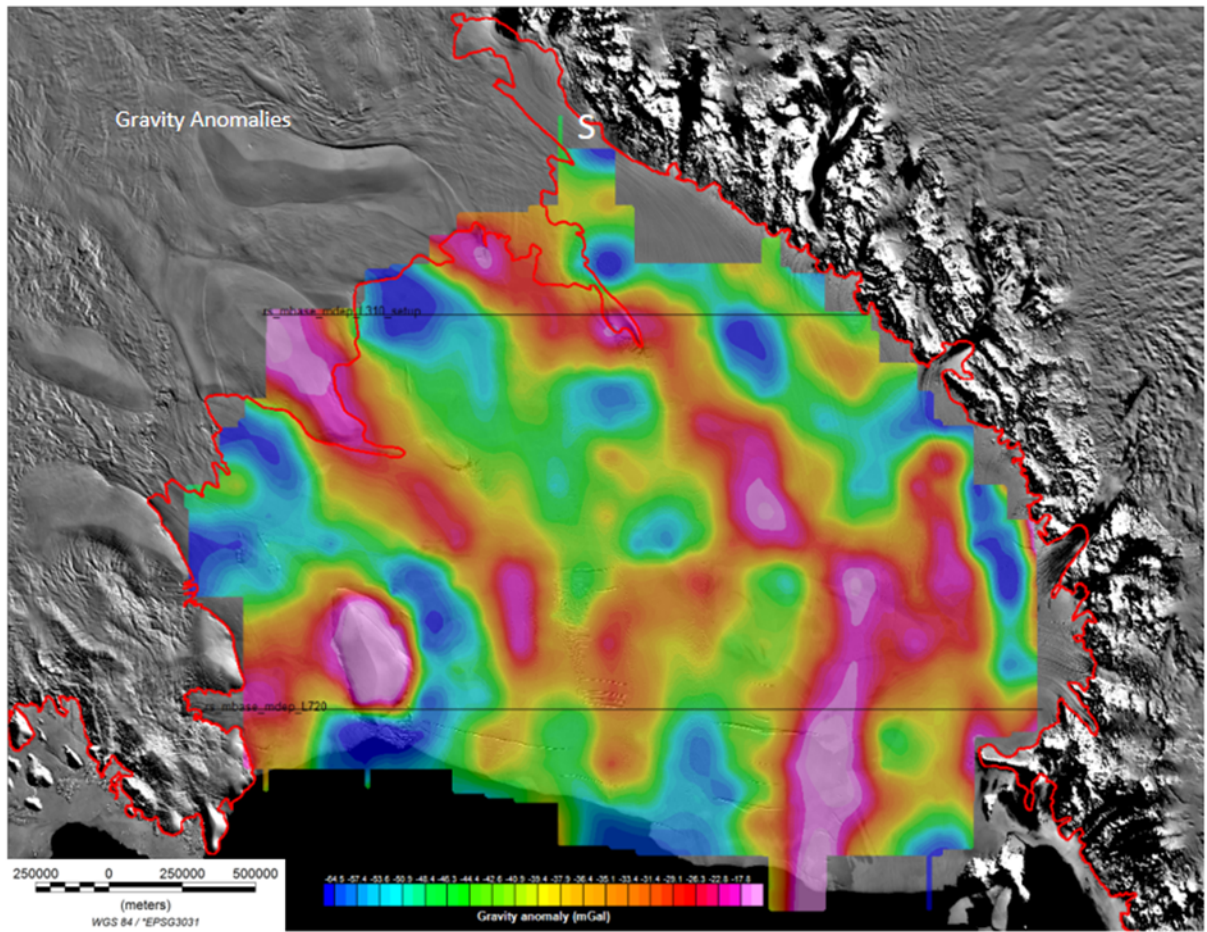


Figure 11: Map of gravity anomalies beneath the Ross Ice Shelf over MODIS imagery. Data is derived from ROSETTA-Ice's 2015-2016 aerogeophysical survey. Values are in mgals; pinks indicate higher values and blues indicate lower values. The data range from -65 mgals to -18 mgals. Black lines are flight lines and transects used for geophysical modeling.

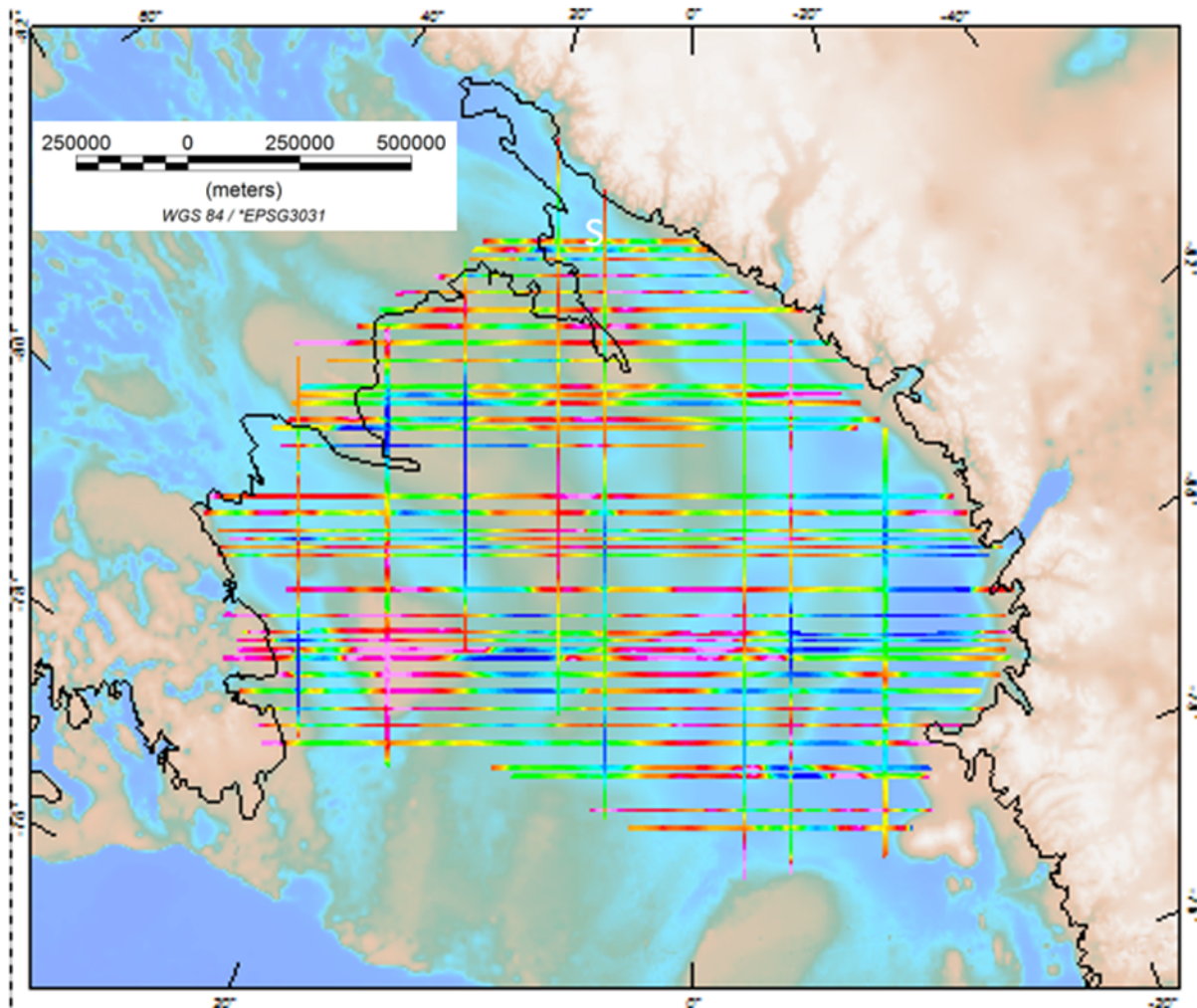


Figure 12: Depth to magnetic basement grid calculated by Wilner et al., (2016) over gravity inverted bathymetry. Blues in the grid are shallow contacts and pinks are deep contacts. Blues in the bathymetry map are basement lows and pinks are basement highs. The black line is the grounding line.

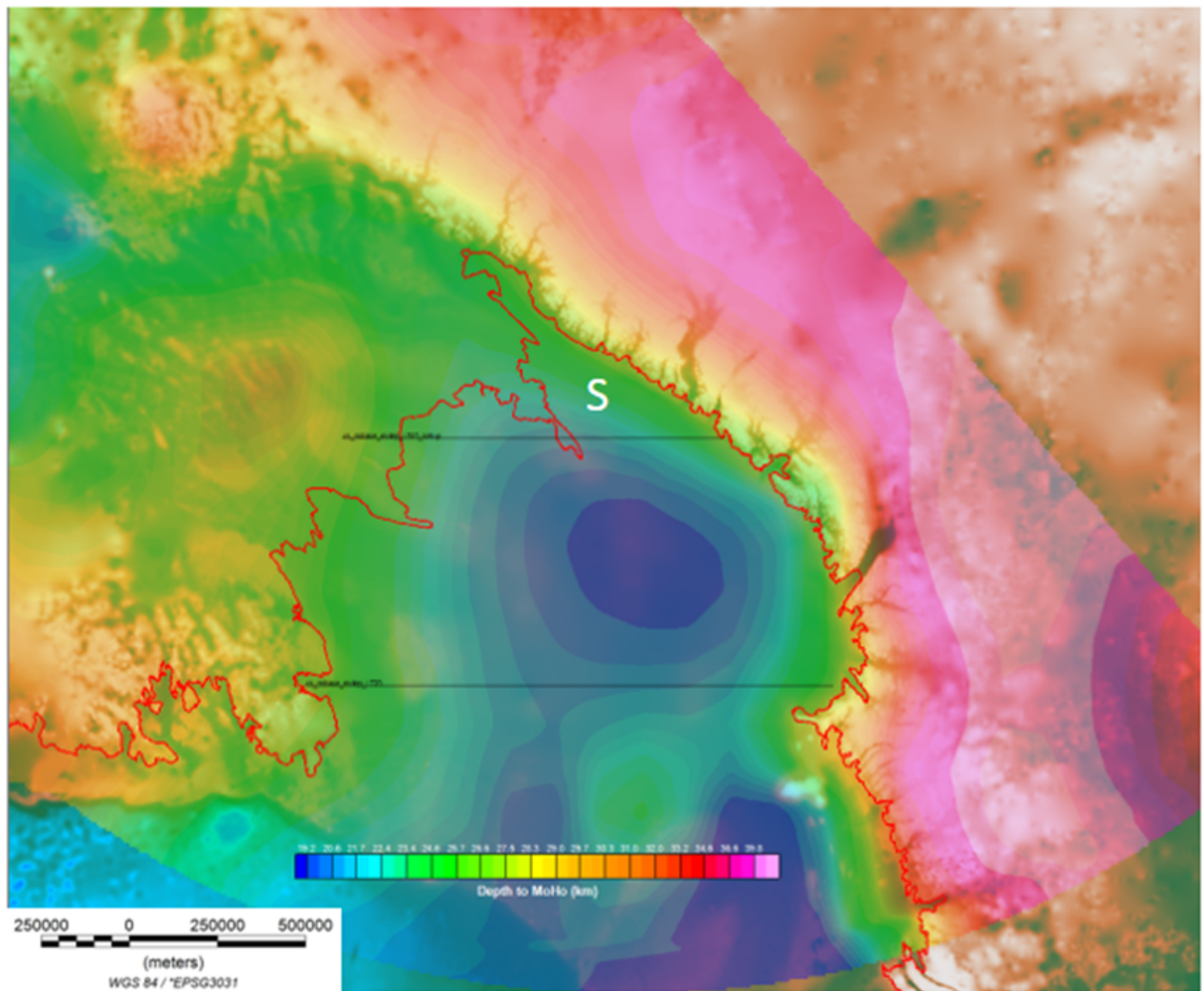


Figure 13: Depth to Moho grid calculated from a model by Chaput et al., (2014). Blues indicate shallow Moho depths and thin crust while pinks reflect deep Moho depths and thick crust. Black lines are survey lines 310 and 720 used for geophysical modeling.

310

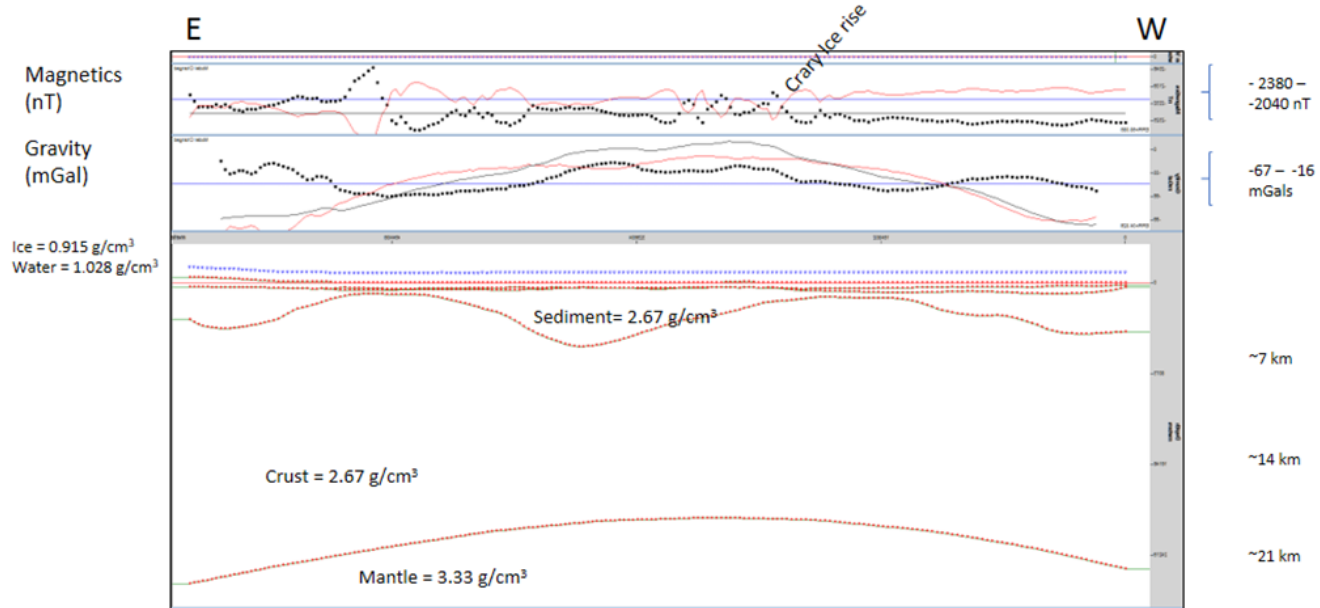
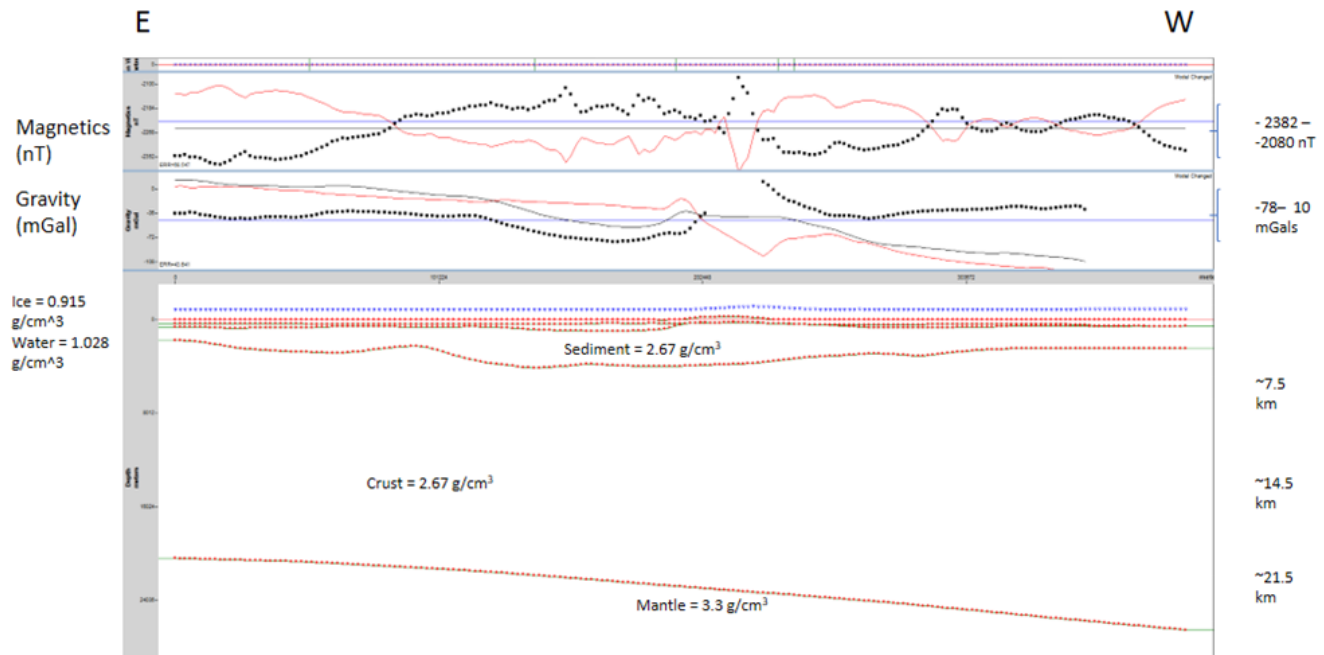


Figure 14: An initial, blank model for survey line 310. The lowest layer (horizon) is the Moho depth (Chaput et al., 2014). The next horizon is the depth to magnetic basement contact (Wilner et al., 2016); above that is the bathymetry horizon, followed by the icebase. The black dots are the observed data that has been collected from the survey; the black line is the calculated data that is produced from inserting polygons and assigning geophysical parameters; the red line is the margin of error. Densities and susceptibility units are in SI. In this initial model, the entire crust has a standard, uniform density of  $2670 \text{ kg/m}^3$  and the mantle a density of  $3300 \text{ kg/m}^3$ . Everything in this profile has a magnetic susceptibility of 0.0 K. The magnetic data show values ranging from -2380 to -2040 nT. Gravity data has a ranges from -67 mgal to -16 mgal.

720



*Figure 15: An initial, blank model for survey line 720. The lowest layer (horizon) is the Moho depth (Chaput et al., 2014). The next horizon is the depth to magnetic basement contact (Wilner et al., 2016); above that is the bathymetry horizon, followed by the icebase. The black dots are the observed data that has been collected from the survey; the black line is the calculated data that is produced from inserting polygons and assigning parameters; the red line is the margin of error. Densities and susceptibility units are in SI. In this initial model, the entire crust has a standard, uniform density of 2670 kg/m<sup>3</sup> and the mantle a density of 3300 kg/m<sup>3</sup>. Everything in this profile has a magnetic susceptibility of 0.0 K (SI). The magnetic data show values ranging from -2382 nT to -2080 nT. Gravity data range from -78 to 10.2 mGals.*

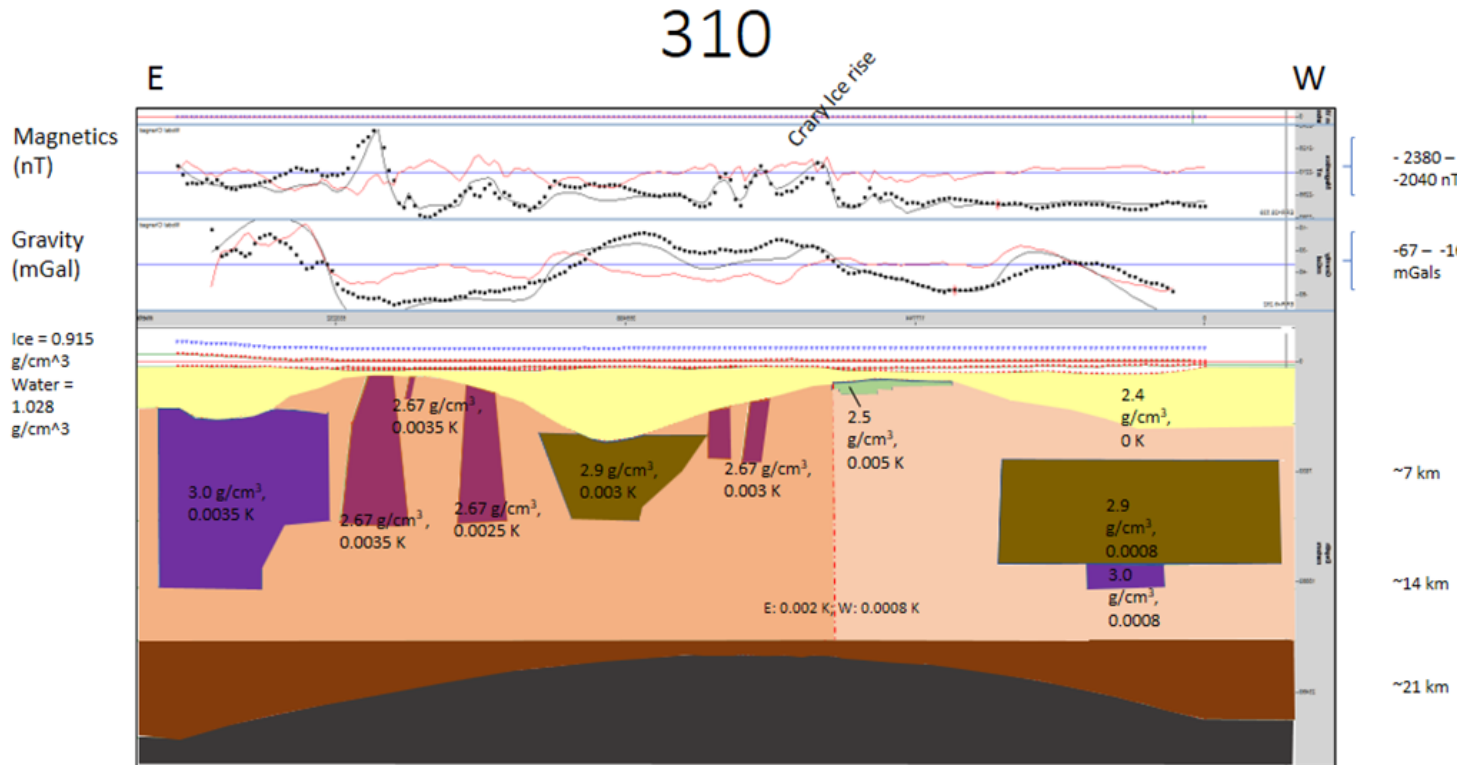
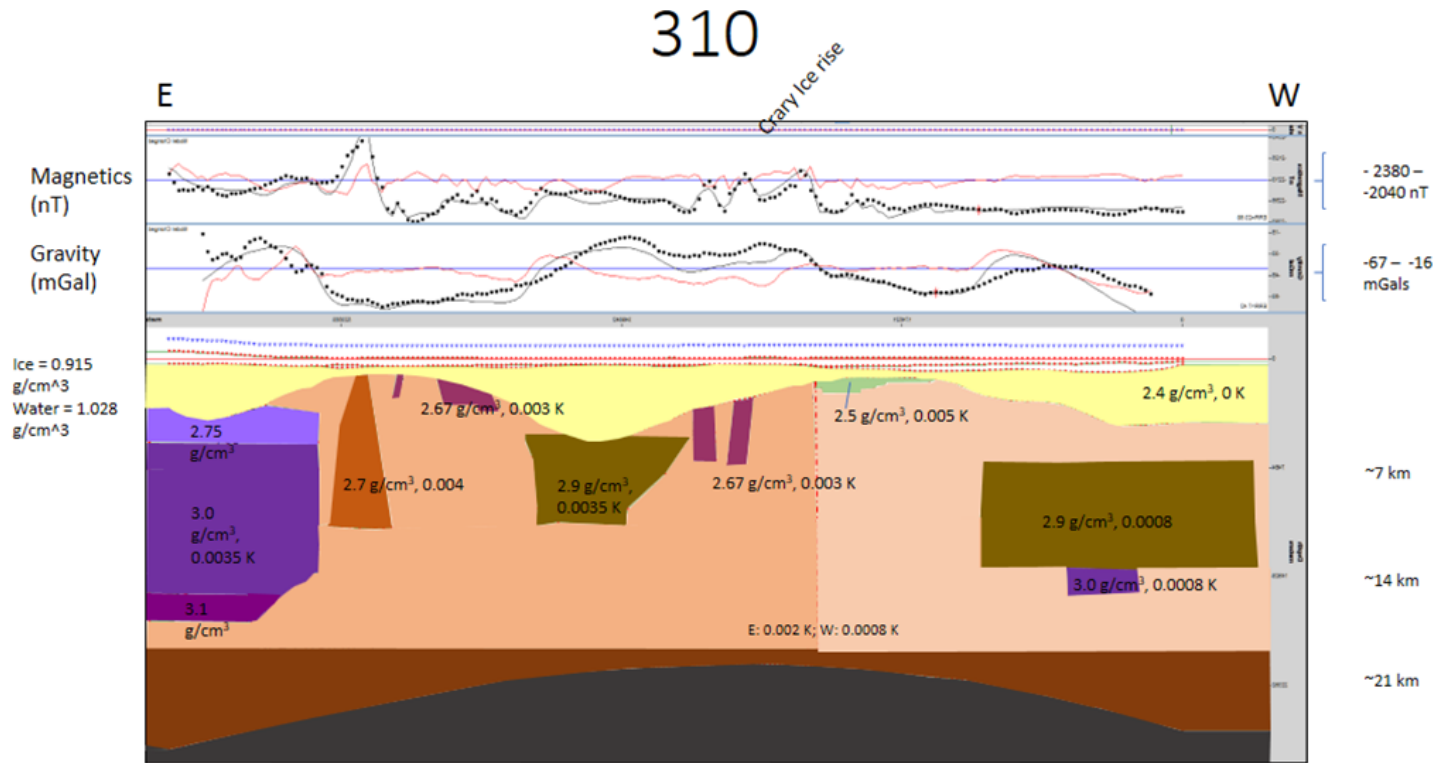


Figure 16: The first iteration of profile 310. Descriptions and rationale for polygons are in the modeling section. Densities and susceptibility units are in SI. Profile from GM-SYS was edited in Microsoft PowerPoint.



*Figure 17: The next iteration of profile 310. Descriptions and rationale for polygons are in the modeling section. Densities and susceptibility units are in SI. Profile from GM-SYS was edited in Microsoft PowerPoint.*

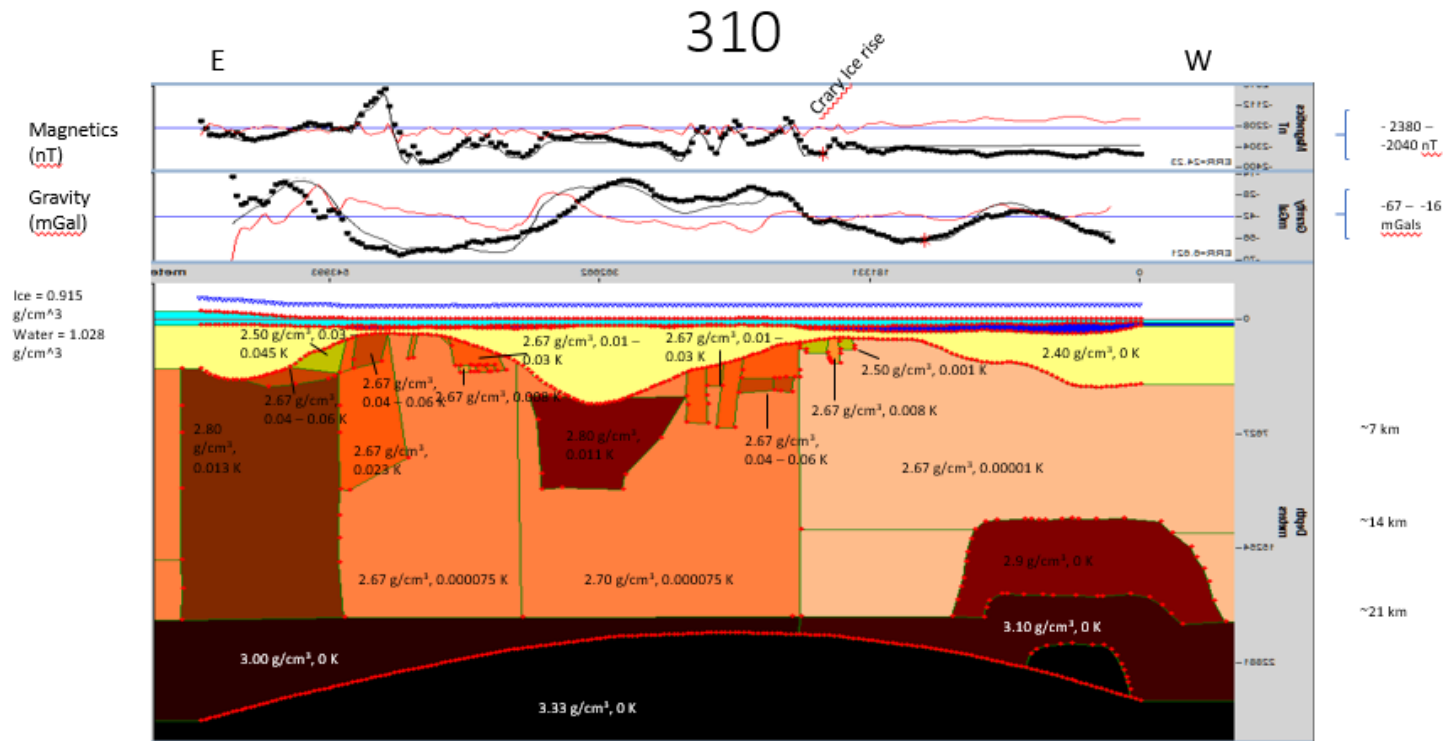


Figure 18: The best iteration thus far of profile 310. Descriptions and rationale for polygons are in the modeling section. Densities and susceptibility units are in SI. Profile from GM-SYS was edited in Microsoft PowerPoint.

720

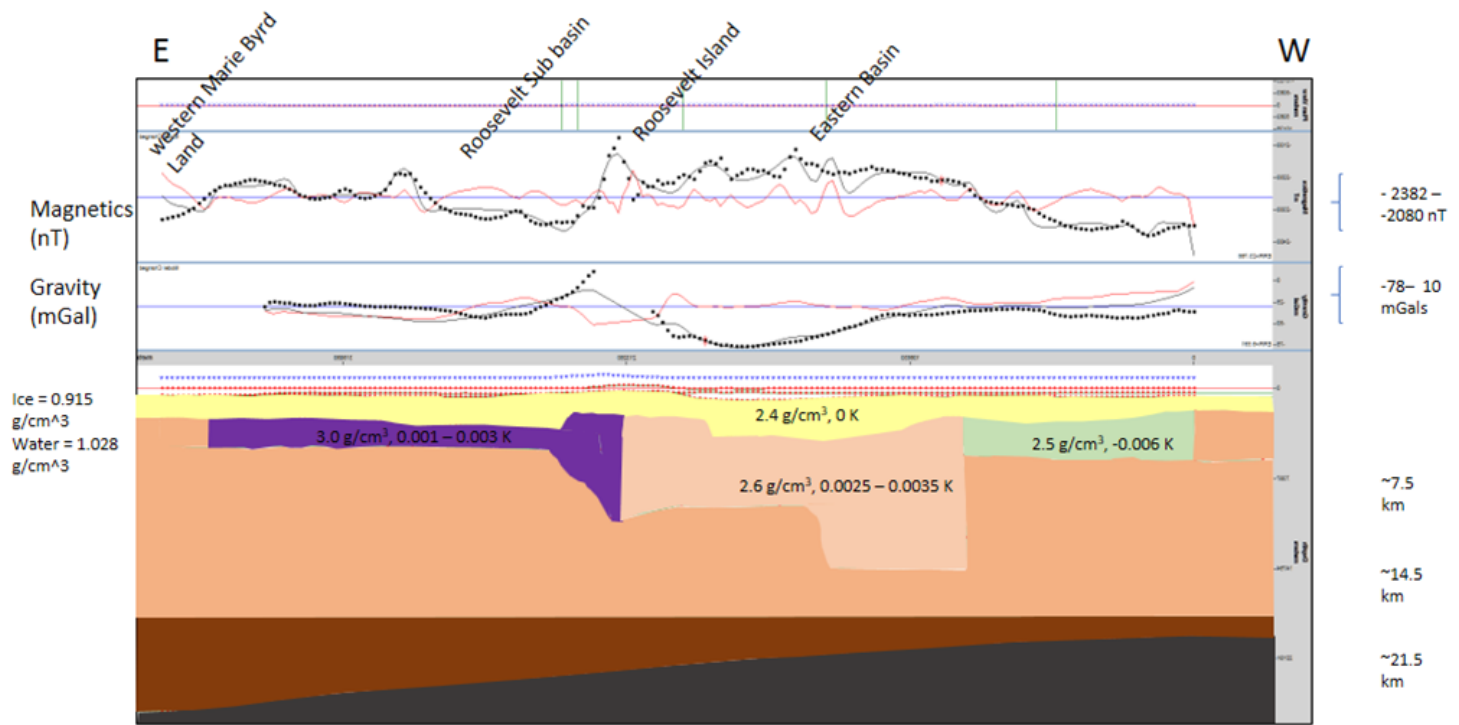


Figure 19: The first iteration of profile 720. Descriptions and rationale for polygons are in the modeling section. Densities and susceptibility units are in SI. Profile from GM-SYS was edited in Microsoft PowerPoint.

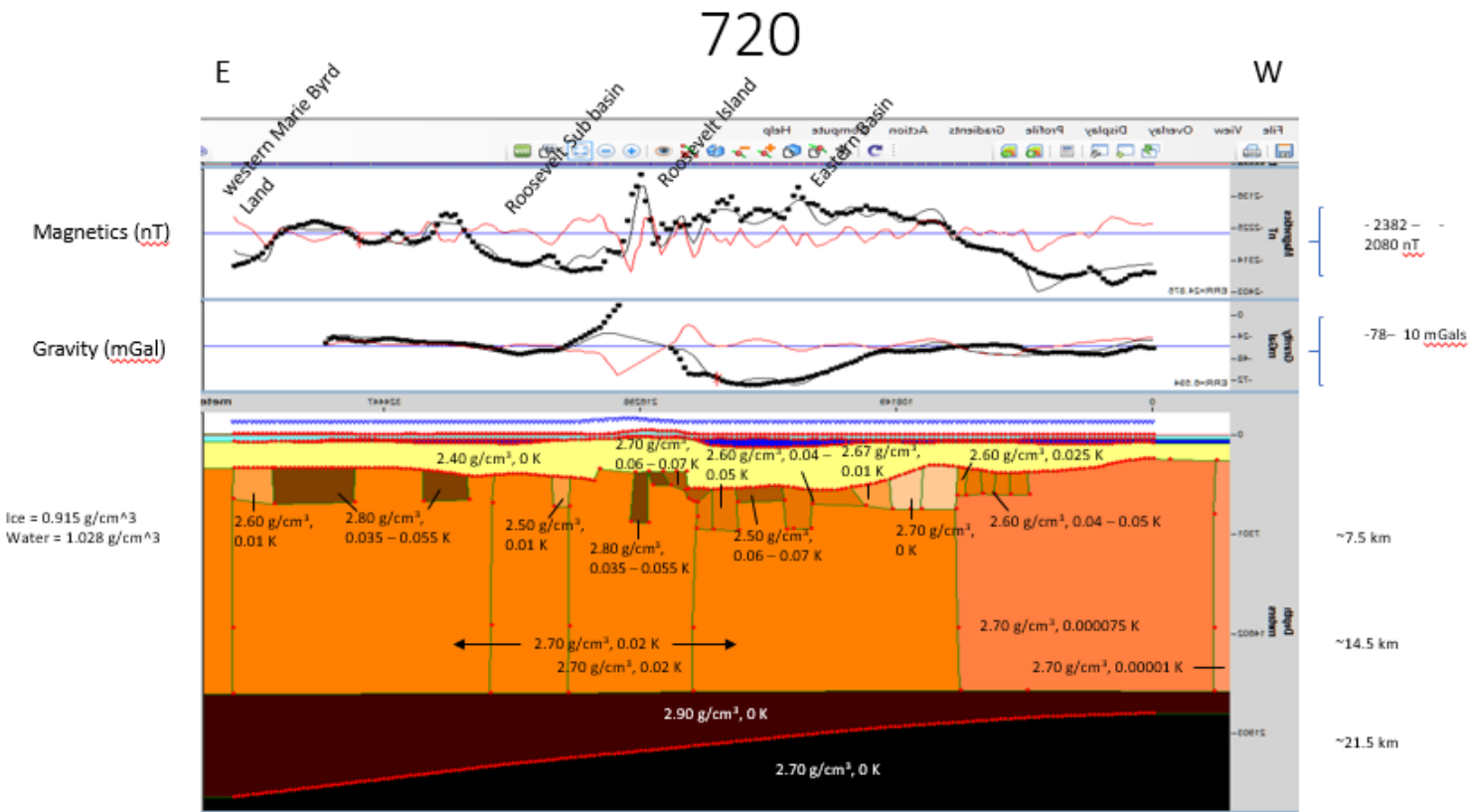


Figure 20: The best iteration thus far of profile 720 Descriptions and rationale for polygons are in the modeling section. Densities and susceptibility units are in SI. Profile from GM-SYS was edited in Microsoft PowerPoint.

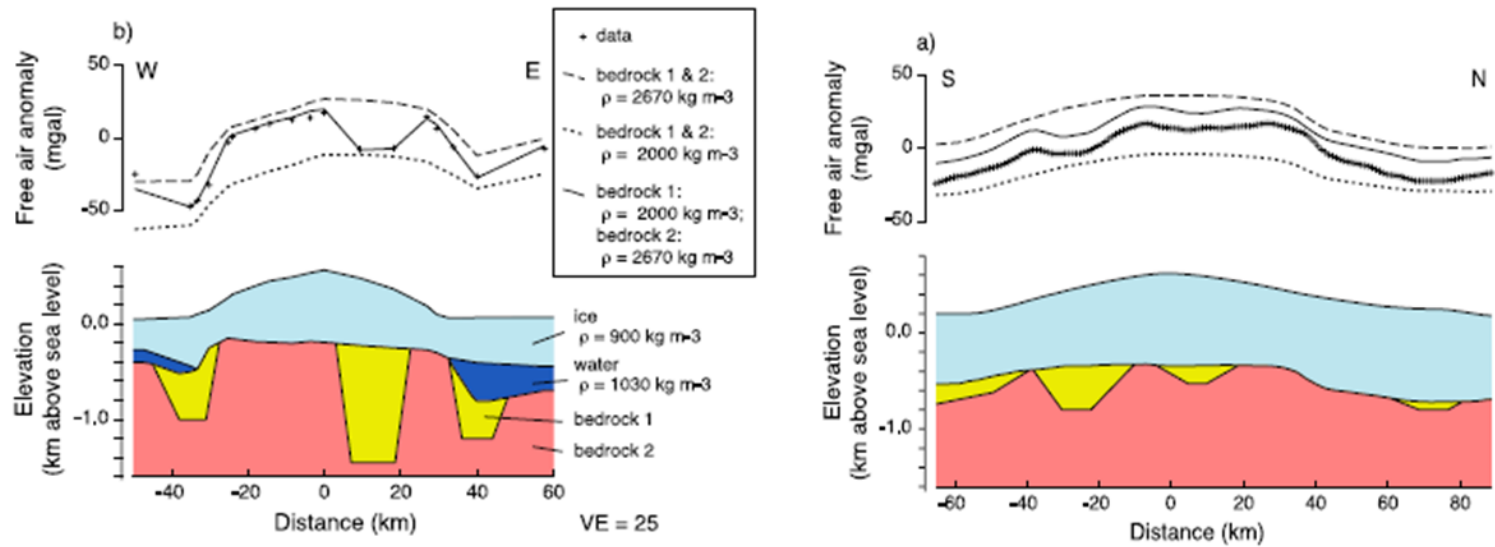


Figure 21: Profiles of Roosevelt Island (left) and Siple Dome (right) modeled using free air gravity anomalies, from *Wilson and Luyendyk*, 2006. Data for RI is from an on-ice survey, while data for Siple Dome is from an airborne survey.

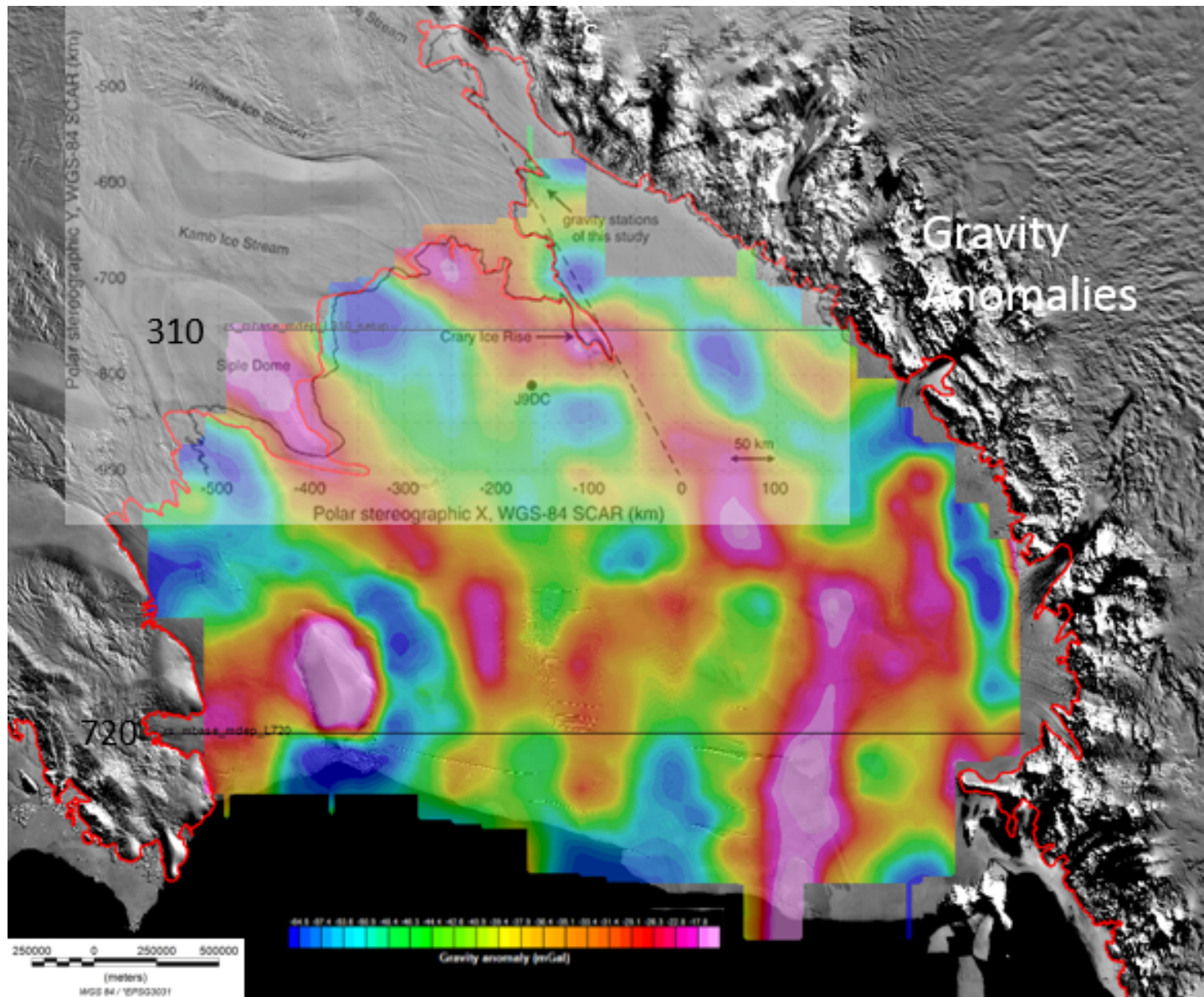


Figure 22: Map of gravity inverted bathymetry overlain on MODIS imagery. A study by Muto et al., 2013 identified the presence of a fault at the base of Whillans ice stream, and modeled the fault extending linearly to the margin of Crary Ice Rise. The figure from Muto et al., 2013 is imposed on this map, and the dashed black line is the proposed fault.

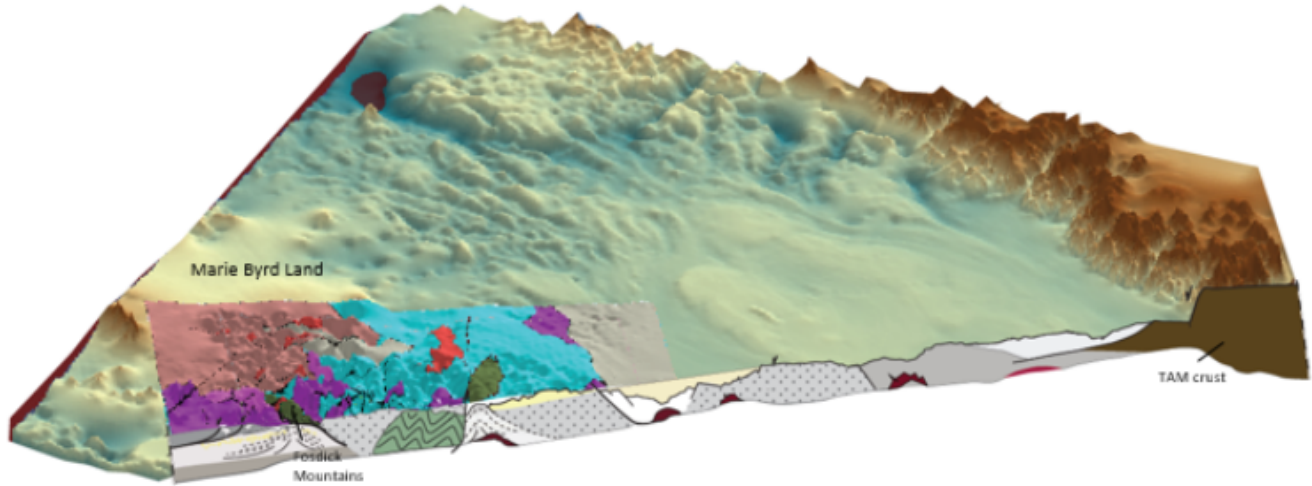


Figure 23: Ross Ice Shelf structural profile (Siddoway et al., 2016), with a subglacial geologic map for western Marie Byrd Land (Elkind et al., 2016), rendered upon Bedmap2 topography. Vertical exaggeration of topography = 10x. The dusty red color indicates Pleistocene (1.4 Ma) basalt or volcanoclastic flow, red shows volcanic necks or mafic dikes, green indicates metamorphic core complexes hosting gneiss domes, yellow/white refers to sediments, purple specifies Ford Granodiorite, light purple signifies Byrd Coast Granite, and brown shows Transantarctic Mountains crust of East Antarctica.

## References

- Behrendt, J.C., Finn, C., Morse, D.L., and Blankenship, D.D., 2007, One hundred negative magnetic anomalies over the West Antarctic Ice Sheet (WAIS), in particular Mt. Resnik, a subaerially erupted volcanic peak, indicated eruption through at least one field reversal, U.S. Geological Survey and the National Academies, 2007-1047.
- Behrendt, J.C., 2013, The aeromagnetic method as a tool to identify Cenozoic magmatism in the West Antarctic Rift System beneath the West Antarctic Ice Sheet — A review; Thiel subglacial volcano as possible source of the ash layer in the WAISCORE, *Tectonophysics*, Volume 585, , Pages 124-136, ISSN 0040-1951, <http://dx.doi.org/10.1016/j.tecto.2012.06.035>.
- Bell, R., Fricker, H., Padman, L., Siddoway, C., and Tinto, K., 2014, Collaborative Research: A systems approach to understanding the Ross Ocean and ice Shelf Environment, and Tectonic setting Through Aerogeophysical surveys and modeling (ROSETTA-ICE), NSF Antarctic Integrated Systems Science, [www.nsf.gov/awardsearch/showAward?AWD\\_ID=1443497](http://www.nsf.gov/awardsearch/showAward?AWD_ID=1443497).
- Bentley, C. R., and Jezek, K. C., 1981, RISS, RISP and RIGGS: Post-IGY glaciological investigations of the Ross Ice Shelf in the U.S. programme, *Journal of the Royal Society of New Zealand*, 11:4, 355-372, DOI: 10.1080/03036758.1981.10423327.
- Bialas, R.W., Buck, W.R., Studinger, M., Fitzgerald, P.G., 2007, Plateau collapse model for the Transantarctic Mountains-West Antarctic Rift System: Insights from numerical experiments, *Geological Society of America*, 35, p. 687-690, doi:10.1130/G23825A.1.
- Beek, P., Cloetingh, S., and Andriessen, P., 1994, Mechanisms of extensional basin formation and vertical motions at rift flanks: Constraints from tectonic modelling and fission-track thermochronology, *Earth and Planetary Science Letters*, v. 121, p. 417 – 433, doi: 10.1016/0012-821X(94)90081-7.
- Chaput, J. Aster, R.C., Huerta, A., Sun, X., Lloyd, A., Wiens, D., Nyblade, A., Anandakrishnan, S., Winberry, J.P. and Wilson, T. (2014): The crustal thickness of West Antarctica.- *Journal of Geophysical Research: Solid Earth*, 119: 1–18.
- Cheever, E., 2015, Developing Mathematical Models of Translating Mechanical Systems, <http://lpsa.swarthmore.edu/Systems/MechTranslating/TransMechSysModel.html>.
- Davey, F. J., Granot, R., Cande, S. C., Stock, J. M., Selvans, M., and Ferraccioli, F., 2016, Synchronous oceanic spreading and continental rifting in West Antarctica, *Geophysical Research Letters*, 43: 6162–6169, doi:10.1002/2016GL069087.
- Decesari, R.C., Wilson, D.S., Luyendyk, B.P., Faulkner, M., 2007, Cretaceous and Tertiary extension throughout the Ross Sea, Antarctica, U.S. Geological Survey and The National Academies, <http://pubs.usgs.gov/of/2007/1047/srp/srp098/of2007-1047srp098.pdf>.
- Elkind, S., Siddoway, C., Cox, S., Morin, P., Smith Lyttle, B., 2016, First digital geological map dataset of Marie Byrd Land: A product of the SCAR GeoMap project, GSA Annual Meeting (abstract), paper 63-20, <https://gsa.confex.com/gsa/2016AM/webprogram/Paper287808.html>.

- Ferraccioli, F., Bozzo, E., and Damaske, D., 2002, Aeromagnetic signatures over western Marie Byrd Land provide insight into magmatic arc basement, mafic magmatism and structure of the Eastern Ross Sea Rift flank, *Tectonophysics*, 139-165.
- Finn, C.A., Pilkington, M., Johnson, S., Cannon, W., Gettings, M., and Roest, W., 2002, Examples of the utility of magnetic anomaly data for geologic mapping, USGS Report, 2002-400, <http://pubs.er.usgs.gov/publication/ofr02400>.
- Fitzgerald, P. G., Baldwin, S. L., 1997, Detachment fault model for Cretaceous extension in the Ross Embayment, Antarctica: Geologic and fission track constraints from DSDP site 270, *The Antarctic Region: Geological Evolution and Processes*, 555-564.
- Fisher, A. T., Mankoff, K. D., Tulaczyk, S. M., and Tyler, S. W., Foley, N., 2015, High geothermal heat flux measured below the West Antarctic Ice Sheet, *Sci. Adv.*, 1500093.
- Fretwell, P., Pritchard, H.D., and 58 others, 2013, Bedmap2:improved ice bed, surface, and thickness datasets for Antarctica, *The Cryosphere*, 7, p. 375-393, doi: 10.5194/tc-7-375-2013.
- Goodge, J. W., and Finn, C. A, 2010, Glimpses of East Antarctica: Aeromagnetic and satellite magnetic view from the central Transantarctic Mountains of East Antarctica, *J. Geophysical Research.*, 115, B09103, doi:10.1029/2009JB006890.
- Huerta, A. D., and Harry, D. L., 2007, The transition from diffuse to focused extension□: Modeled evolution of the West Antarctic Rift system, *Earth and Planetary Science Letters*, 255 133–147, doi:10.1016/j.epsl.2006.12.011.
- Jacobs, S. S., Jenkins, A., Giulivi, C. F., & Dutrieux, P. 2011, Stronger ocean circulation and increased melting under Pine Island Glacier ice shelf. *Nature Geoscience*, 4(8), 519–523. <https://doi.org/10.1038/ngeo1188>.
- Joughin, I., Alley, R.B., and Holland, D.M., 2005, Ice-Sheet Response to Oceanic Forcing, *Science*, 338: 1095-9203.
- Justman, B.P., 2016, Gravity and Magnetic Analysis of Subsurface Geologic Structures in the Granite Falls Quadrangle, Washington, Colorado College, Department of Geology.
- Karner, G.D., Studinger, M., and Bell, R.E., 2005, Gravity anomalies of sedimentary basins and their mechanical implications: Application to the Ross Sea basins, West Antarctica, *Earth and Planetary Science Letters*, 235: 3-4, doi:10.1016/j.epsl.2005.04.016.
- Lamont Doherty Earth Observatory, Columbia University, 2017, An Integrated Ice Imaging System for LC-130s, <http://www.ldeo.columbia.edu/res/pi/icepod/Instruments.html>.
- LeMasurier, W.E., and Rocchi, S., 2005, Terrestrial Record of Post-Eocene Climate History in Marie Byrd Land, West Antarctica, *Geografiska Annaler: Series A, Physical Geography*, 87: 1, DOI: 10.1111/j.0435-3676.2005.00244.x.
- Lillie, R., 1999, Whole Earth Geophysics an Introductory Textbook for Geologists and Geophysicists: Upper Saddle River, N.J., Prentice Hall.

- Luyendyk, B. P., Wilson, D. S., and Decesari, R., 2002, New maps of gravity and bedrock-bathymetry of the Ross Sea sector of Antarctica, *Eos Trans. AGU*, 83(47), Fall Meet. Suppl., Abstract T12D-1339.
- Luyendyk, B. P., Wilson, D. S., Siddoway, C. S., & Land, B. 2003, Eastern margin of the Ross Sea Rift in western Marie Byrd Land, Antarctica: Crustal structure and tectonic development. <https://doi.org/10.1029/2002GC000462>.
- McFadden R., C. S. Siddoway, C. Teyssier, and C. M. Fanning, 2010, Cretaceous oblique extensional deformation and magma accumulation in the Fosdick Mountains migmatite-cored gneiss dome, West Antarctica, *Tectonics*, v. 29, TC4022, doi:10.1029/2009TC002492.
- Monastero, F.C., Miller, J. S., Unruh, J. R., Adams, M. C., & Richards-Dinger, K., 2005, The Coso geothermal field□: A nascent metamorphic core complex, *GSA Bulletin*, (11), 1534–1553. <https://doi.org/10.1130/B25600.1>.
- Morrison, F., Gasperikova, E., 2016, The Berkeley course in applied geophysics. <https://www.eoas.ubc.ca/ubcgif/iag/foundations/properties/density.htm>.
- Muto, A., Christianson, K., Horgan, H. J., Anandakrishnan, S., & Alley, R. B. (2013). Bathymetry and geological structures beneath the Ross Ice Shelf at the mouth of Whillans Ice Stream , West Antarctica , modeled from ground-based gravity measurements, 118, 4535–4546. <https://doi.org/10.1002/jgrb.50315>.
- National Oceanic and Atmospheric Administration, 2017, Magnetic Field Calculators, <https://www.ngdc.noaa.gov/geomag-web/#igrfwmm>.
- Pankhurst, R.J., Ireland, T. R., Weaver, S. D., Bradshaw, J. D., Spautorey, B. C., Marie, A., & Land, B, 1998, Geochronology and geochemistry of pre-Jurassic superterrane in Marie Byrd Land, Antarctica, *Journal of Geophysical Research*, 103(97), 2529–2547.
- Paulsen, T.S., Wilson, T.J., 2017, Evolution of Neogene volcanism and stress patterns in the glaciated West Antarctic, *Journal of the Geological Society, London*, 167, 401–416. doi:10.1144/0016-76492009-044.
- Peters, L. E., Anandakrishnan, S., Alley, R.B., Winberry, J.B., Voigt, D.E., Smith, A.M., and Morse, D.L., 2006, Subglacial sediments as a control on the onset and location of two Siple Coast ice streams, West Antarctica, *J. Geophys. Res.*, 111: B01302, doi:10.1029/2005JB003766.
- Polar Geospatial Center (PGC). Antarctica [map]. 2015. 1:5,500,000. [http://www.pgc.umn.edu/mapsantarctic/id/ANT\\_REF-MP2015-001](http://www.pgc.umn.edu/mapsantarctic/id/ANT_REF-MP2015-001).
- Rey, P. F., & Müller, R. D. (2010). Fragmentation of active continental plate margins owing to the buoyancy of the mantle wedge. *Nature Geoscience*, 3(4), 257–261. <https://doi.org/10.1038/ngeo825>.
- Rignot, E., J. Mouginot, M. Morlighem, H. Seroussi, and B. Scheuchl (2014), Widespread, rapid grounding line retreat of Pine Island, Thwaites, Smith, and Kohler glaciers, West Antarctica, from 1992 to 2011, *Geophys. Res. Lett.*, 41, 3502–3509, doi:10.1002/2014GL060140.
- Rudnick, R. R., and Gao, S., 2003, Composition of the Continental Crust, *Treatise on Geochemistry*, v. 3, p. 1 – 64, doi: 10.1016/B0-08-043751-6/03016-4.

Siddoway, C.S; Richard, S.; Fanning, C.M.; and Luyendyk, B. P., 2004, Origin and emplacement mechanisms for a middle Cretaceous gneiss dome, Fosdick Mountains, West Antarctica, in Whitney, D.L., Teyssier, C.T., and Siddoway, C., eds., Gneiss domes in orogeny, GSA Special Paper 380, p. 267–294.

Siddoway, C., Sass, C.L., Esser, R.P., 2005, Kinematic history of western Marie Byrd Land, West Antarctica: direct evidence from Cretaceous mafic dykes, Geological Society, London, Special Publications 2005, v. 246, doi: 10.1144/GSL.SP.2005.246.01.17.

Siddoway, C., 2008, Tectonics of the West Antarctic rift system: New light on the history and dynamics of distributed intracontinental extension (invited paper) in Cooper, A. et al., Antarctica: A Keystone in a Changing World, National Academy of Sciences, Washington, D.C., pp. 91-114. <https://pubs.er.usgs.gov/publication/ofr20071047KP09>.

Siddoway, C., 2016, Geology of West Antarctica (invited chapter, submitted), in Kleinschmidt, G., ed., Geology of the Antarctic Continent. Stuttgart: Gebrüder Borntraeger Verlagsbuchhandlung.

Siddoway, C., Elkind, S., Cox, S., Smith Lyttle, B., 2016, Antarctic GeoMAP for Marie Byrd Land: A digital map of exposed and subglacial geology and surficial glacial deposits, XXXIV SCAR Biennial Meeting and Open Science Conference, Kuala Lumpur, Malaysia (22-26 August).

Sorlien, C. C., Studies, C., Santa, C., Barbara, S., Luyendyk, B. P., Wilson, D. S., ... Land, M. B., 2007, Oligocene development of the West Antarctic Ice Sheet recorded in eastern Ross Sea strata, (5), 467–470. <https://doi.org/10.1130/G23387A.1>.

Studinger, M., Bell, R. E., Buck, W. R., Karner, G. D., and Blankenship, D. D., 2004, Sub-ice geology inland of the Transantarctic Mountains in light of new aerogeophysical data, Earth and Planetary Science Letters, v. 220, doi: 10.1016/S0012-821X(04)00066-4.

Tinto, K., Bell, R., Cochran, J., Charles, K., and Burton, B., 2016, Improved bathymetry resolution in the Ross Sea from aerogravity and magnetics: examples from Operation IceBridge, Lamont-Doherty Earth Observatory.

Vogel, S.W., Tulaczyk, S., Carter, S., Renne, P., Turrin, B., and Grunow, A., 2006, Geologic constraints on the existence and distribution of West Antarctic subglacial volcanism, Geophys. Res. Lett., 33, L23501, doi:[10.1029/2006GL027344](https://doi.org/10.1029/2006GL027344).

Wilner, J., Bell, R., and Tinto, K., 2016, Magnetically Derived Distribution of Sediments Beneath the Ross Ice Shelf, Antarctica, American Geophysical Union poster.

Wilson, D.S., and Luyendyk, B.P., 2006, Bedrock platforms within the Ross Embayment, West Antarctica: Hypotheses for ice sheet history, wave erosion, Cenozoic extension, and thermal subsidence, Geochemistry Geophysics Geosystems, 7: 12, doi:10.1029/2006GC001294.

Worthington, L. & 9 others, 2016, Crustal structure of the Bighorn Mountains region: Precambrian Influence on Laramide shortening and uplift in north-central Wyoming, *Tectonics*, 35, doi:10.1002/2015TC003840.

Yakymchuk, C., Brown, C.R., Brown, M., Siddoway, C.S., Fanning, C.M. and Korhonen, F.J., 2015, Paleozoic evolution of West Marie Byrd Land, West Antarctica: Geological Society of America Bulletin, doi:10.1130/B31136.1.